



Drivers of phytoplankton bloom interannual variability in the Amundsen and Pine Island Polynyas

Guillaume Liniger^{1,2}, Delphine Lannuzel^{1,3,4}, Sébastien Moreau⁵, Michael S. Dinniman⁶, and Peter G. Strutton^{1,3}

¹Institute for Marine and Antarctic Studies, University of Tasmania, Hobart, Australia

²Monterey Bay Aquarium Research Institute, Moss Landing, CA, USA

³Australian Centre for Excellence in Antarctic Science, University of Tasmania, Hobart, Australia

⁴Australian Antarctic Program Partnership, University of Tasmania, Hobart, Australia

⁵Norwegian Polar Institute, Tromsø, Norway

⁶Center for Coastal Physical Oceanography, Old Dominion University, Norfolk, VA, USA

Correspondence: Guillaume Liniger (liniger@mbari.org)

Received: 1 July 2025 – Discussion started: 25 July 2025

Revised: 8 January 2026 – Accepted: 12 January 2026 – Published: 26 January 2026

Abstract. The Amundsen Sea Embayment (ASE) experiences both the highest ice shelf melt rates and the highest biological productivity in West Antarctica. Using 19 years of satellite data and modelling output, we investigate the long-term influence of environmental factors on the phytoplankton bloom in the Amundsen Sea (ASP) and Pine Island (PIP) polynyas. We test the prevailing hypothesis that changes in ice shelf melt rate could drive interannual variability in the polynyas' surface chlorophyll-*a* (chl *a*) and Net Primary Productivity (NPP). We find that the interannual variability and long-term change in glacial meltwater may play an important role in chl *a* variance in the ASP, but not for NPP. Glacial meltwater does not explain the variability in neither chl *a* or NPP in the PIP, where light and temperature are the main drivers. We attribute this to potentially greater amount of iron-enriched meltwater brought to the surface by the meltwater pump downstream of the PIP, and the coastal ocean circulation accumulating and transporting iron towards the ASP.

1 Introduction

Coastal polynyas are open ocean areas formed by strong katabatic winds pushing sea ice offshore (Morales Maqueda, 2004). They are the most biologically productive areas in the Southern Ocean (SO) relative to their size (Arrigo et al., 1998). This high biological productivity contrasts sharply

with the rest of the SO, where low iron (Fe) and light availability generally co-limit phytoplankton growth (Boyd et al., 2007). In West Antarctica, the Amundsen Sea Embayment (ASE) hosts two of the most productive Antarctic polynyas: The Pine Island Polynya (PIP) and Amundsen Sea Polynya (ASP) (Arrigo and van Dijken, 2003).

The phytoplankton community in the ASE is generally dominated by *Phaeocystis antarctica* (Lee et al., 2017; Yager et al., 2016), which is adapted to low iron availability and variable light conditions, and forms large summer blooms (Alderkamp et al., 2012; Yager et al., 2016). Diatoms like *Fragilariopsis* sp. and *Chaetoceros* sp. are also present, often becoming more important near the sea-ice edge or under shallow, stratified mixed layers where silicic acid (Si) and iron are more available (Mills et al., 2012). In exceptional years, such as 2020, diatoms like *Dactyliosolen tenuijunctus* replaced *P. antarctica* as the dominant taxon, driven by anomalously shallow mixed layers and sufficient Fe-Si supply (Lee et al., 2022). This dynamic balance highlights how light, nutrient supply, and stratification control community composition in these highly productive and complex Antarctic systems.

The ASE is also the Antarctic region experiencing the highest mass loss from the Antarctic ice sheet. It has been undergoing increased calving, melting, thinning and retreat over the past three decades (Paolo et al., 2015; Rignot et al., 2013; Rignot et al., 2019; Shepherd et al., 2018). In the ASE, this ice loss is mainly through enhanced basal melting of the

ice shelves. This is attributed to an increase in wind-driven Circumpolar Deep Water (CDW) fluxes and ocean heat content intruding onto the continental shelf through deep troughs such as the Pine Island and Dotson-Getz, and flowing into the ice shelves cavities (Dotto et al., 2019; Jacobs et al., 2011; Pritchard et al., 2012). There, warm waters fuel intense basal melt of the Pine Island, Thwaites, and Getz ice shelves, and returns as a fresher, colder outflow that can strengthen stratification (Jenkins et al., 2010; Ha et al., 2014). The PIP and ASP differ in their exposure to CDW and in local circulation: the ASP is more strongly influenced by upwelled modified CDW (mCDW) and glacial meltwater inputs, whereas in the PIP, the deep mCDW retains more of its original offshore characteristics, with vertical exchange only significantly occurring beneath the ice shelves, leading to a more stratified and less directly ventilated surface layer (Assmann et al., 2013; Dutrieux et al., 2014). These hydrographic contrasts can shape the timing and magnitude of phytoplankton blooms and nutrient dynamics across the two polynyas.

Melting ice shelves can explain about 60 % of the biomass variance between all Antarctic polynyas, suggesting that they are the primary supplier of dissolved iron (dFe) to coastal polynyas (Arrigo et al., 2015), and can directly or indirectly contribute to regional marine productivity (Bhatia et al., 2013; Gerringa et al., 2012; Hawkings et al., 2014; Herraiz-Borreguero et al., 2016). The strong melting of ice shelves can release significant quantities of freshwater at depth (Biddle et al., 2017), resulting in a strong overturning within the ice shelves cavity, called the meltwater pump (St-Laurent et al., 2017). Modelling efforts have identified both resuspended Fe-enriched sediments and CDW entrained to the surface by the meltwater pump as the two primary sources of dFe to coastal polynyas, providing up to 31 % of the total dFe, compared to 6 % for direct ice shelves input (Dinniman et al., 2020; St-Laurent et al., 2017). Other drivers such as sea-ice coverage (and associated increases in light and dFe availability when sea ice retreats), or winds have also been shown to impact primary productivity in polynyas (Park et al., 2019; Park et al., 2017; Viallancourt et al., 2003).

The key question of how glacial meltwater variability may impact biological productivity in the ASE has previously been raised during the ASPIRE program (Yager et al., 2012). During the expedition, a significant supply of melt-laden Fe-enriched seawater to the central euphotic zone of the ASP was observed, potentially explaining why this area is the most biologically productive in Antarctica (Randall-Goodwin et al., 2015; Sherrell et al., 2015). Other studies in the Western Antarctic Peninsula and East Antarctica showed that the meltwater pump process was also responsible for natural Fe supply to the surface, increasing primary productivity (Cape et al., 2019; Tamura et al., 2023).

In this study, we investigate the long-term relationship between the main environmental factors of the ASE and the surface biological productivity, with a focus on ice shelves melting. A demonstrated relationship between glacial meltwater

and phytoplankton growth would have far-reaching consequences for regional productivity in coastal Antarctica, and possibly offshore, over the coming decades under expected climate change scenarios (Meredith et al., 2019). We test the hypothesis that changes in glacial meltwater are linked to the surface ocean primary productivity variability observed over the last two decades. We use a combination of satellite (ocean color and ice shelf melting rate), climate re-analysis, and model data spanning 1998 to 2017.

2 Material and Methods

2.1 Study area and polynya mapping

We focus on the PIP and ASP in the ASE in West Antarctica (Fig. 1). The ASE is comprised of several ice shelves and glaciers, including: Abbot (Abb), Cosgrove (Cs), Pine Island (PIG), Thwaites (Tw), Crosson (Cr), Dotson (Dt) and Getz (Gt). The PIG and Thwaites have received significant attention in recent years due to their potentially large contribution to sea level rise (Rignot et al., 2019; Scambos et al., 2017). Along with the Crosson and Dotson ice shelves, the PIG and Thwaites are undergoing the highest melt rate, which is expected to increase under climate change scenarios (Naughten et al., 2023; Paolo et al., 2023). The polynyas' boundaries were determined using a 15 % sea-ice concentration (SIC) mask (Moreau et al., 2015; Stammerjohn et al., 2008) for every 8 d period from June 1998 to June 2017 to accurately represent the size of the polynyas through time.

2.2 Satellite ocean surface chlorophyll- α and net primary productivity

We obtained level-3 satellite surface chlorophyll- α concentration (chl α) with spatial and temporal resolution of 0.04° and 8 d from the European Space Agency (ESA) Glob-color project. We used the CHL1-GSM (Garver-Siegel-Maritorena) (Maritorena and Siegel, 2005) standard Case 1 water merged products consisting of the Sea-viewing Wide Field-of-view (SeaWiFS), Medium Resolution Imaging Spectrometer (MERIS), Moderate Resolution Imaging Spectroradiometer (MODIS-A) and Visible Infrared Imaging Suite sensors (VIIRS). We chose to perform our analysis with the merged GlobColour product, which has been widely applied and tested in Southern Ocean and coastal Antarctic studies (Ardyna et al., 2017; Sari El Dine et al., 2025; Golder and Antoine, 2025; Nunes et al., 2025), to increase our spatial and temporal coverage.

We estimated phytoplankton bloom phenology metrics following the Kauko et al. (2021) method. Firstly, for a given 8 d period, we applied a spatial 3×3 pixels median filter to reduce gaps in missing data. Then, if a pixel was still empty, we applied the average chl α of the previous and following week to fill the data gap. Data were smoothed using a 4-point moving median (representing a month of data). For each pixel, the

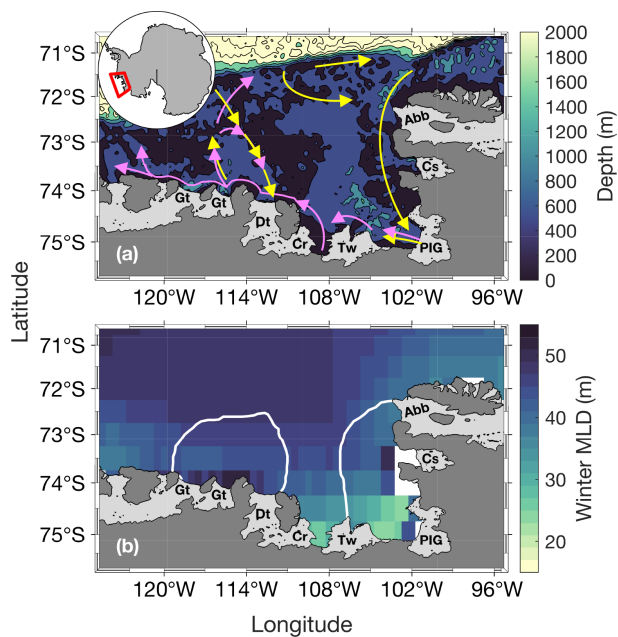


Figure 1. Study area. Panel (a) shows the bathymetry (from ETOPO1; Amante and Eakins, 2009) and panel (b) shows the climatological April–September (that we call winter) mixed-layer depth (MLD) from 1998 to 2016 ($n = 114$). Panel (a) shows a simplified schematic of the local deep ocean circulation (\sim below 400 m, yellow arrows) and upper glacial meltwater/sediments/circumpolar deep water sourced dFe pathways (magenta arrows), which follows the local upper ocean circulation. Schematic adapted from St-Laurent et al. (2017). The white lines in panel (b) represent the climatological summer polynyas' boundaries for the Amundsen (ASP; left) and Pine Island (PIP; right) polynyas. The dark grey area is mainland Antarctica. Light grey areas indicate floating ice shelves and glaciers: Abbot (Abb), Cosgrove (Cs), Pine Island Glacier (PIG), Thwaites (Tw), Crosson (Cr), Dotson (Dt) and Getz (Gt).

threshold for the bloom detection was based on 1.05 times the annual median. The threshold method is frequently used (Racault et al., 2012; Siegel et al., 2002) and proven reliable at higher latitudes (Marchese et al., 2017; Soppa et al., 2016; Thomalla et al., 2023). We then determined 5 main bloom metrics. The bloom start (BS) is defined as the day where chl *a* first exceeds the threshold for at least 2 consecutive 8 d periods. Conversely, the bloom end is the day where chl *a* first falls below the threshold for at least 2 consecutive 8 d periods. The bloom duration (BD) is the time elapsed between bloom start and bloom end. The bloom mean chl *a* (BM) and bloom maximum chl *a* are respectively the average and maximum chl *a* value calculated during the bloom. Each year is centered around austral summer, from 10 June year n (day 1) to 9 June year $n + 1$ (day 365 or 366). We also averaged our 8 d data to monthly data to perform a spatial correlation analysis (see Sect. 2.6).

We note that satellite ocean-colour chl *a* algorithms (including the GlobColour merged product used here) are globally tuned and may underperform in optically complex waters (e.g., with elevated dissolved organic matter or suspended sediments, “Case 2”). In the ASP, past work (Park et al., 2017) showed that satellite chl *a* climatologies reflect broad seasonal patterns that are consistent with in situ measurements of phytoplankton biomass and photophysiology, but there is limited data from regions immediately adjacent to glacier fronts or during times of strong meltwater input. Thus, while we consider satellite chl *a* to be useful for capturing spatial and temporal variability at polynya scale, uncertainty likely increases in optically complex zones near glacier margins or during low-light periods, and needs to be considered while interpreting results.

Eight-day satellite derived Net Primary Productivity (NPP) data with $1/12^\circ$ spatial resolution, spanning 1998–2017 using the Vertically Generalized Production Model (Behrenfeld and Falkowski, 1997) were obtained from the Oregon State University website. The VGPM model is a chlorophyll-based approach and relies on the assumption that NPP is a function of chl *a*, influenced by light availability and maximum daily net primary production within the euphotic zone. SeaWiFS-based NPP data span 1998–2009, MODIS-based data span 2002–2017. To increase spatial and temporal coverage, we averaged SeaWiFS and MODIS from 2002 to 2009, where there was valid data for both in a pixel. NPP data were also monthly averaged and used to compare with chl *a* spatial and temporal patterns.

We caution that our study focuses on surface productivity, and satellites cannot detect under-ice phytoplankton, sea-ice algal blooms, or deeper productivity, therefore likely underestimating total primary productivity (Ardyna et al., 2020; Boles et al., 2020; Douglas et al., 2024; McClish and Bushinsky, 2023; Stoer and Fennel, 2024).

2.3 Ice shelves volume flux

We used the latest ice shelf basal melt rate estimates from Paolo et al. (2023). These estimates are derived from satellite radar altimetry measurements of ice shelves height, and produced on a 3 km grid every 3 months, with an effective resolution of ~ 5 km. For this study, our basal melt record spans June 1998 to June 2017. We calculated ice shelves volume flux rate for every gridded cell by multiplying the basal melt rate by the cell area. Data were summed for each ice shelf for a 3-month period. A 5-point (15 months) running mean was applied to reduce noise, such as spurious effects induced by seasonality on radar measurements over icy surfaces (Paolo et al., 2016), and data were temporally averaged from October to March to match the SO phytoplankton growth season (Arrigo et al., 2015), providing yearly mean values. The Abbot, Cosgrove, Thwaites, PIG, Crosson, Dotson and Getz ice shelves were used to calculate a single total meltwater volume flux (TVFall) for the ASE to investigate

the link with surface chl *a* and NPP. We also investigated the relationship between each polynyas' productivity and their closest ice shelf. The Abbot, Cosgrove, PIG and Thwaites ice shelves were used to calculate the flux rate in the PIP (TVFpip) while the Thwaites, Crosson, Dotson and Getz ice shelves were chosen for the ASP (TVFasp). The Thwaites was used in both due to its central position between the two polynyas. We thereafter use the term glacial meltwater which defines meltwater resulting from ice shelf melting.

2.4 Simulated dFe distribution

The spatial distribution of dFe from different sources in the embayment was investigated from Dinniman et al. (2020) model output. The model used is a Regional Ocean Modelling System (ROMS) model, with a 5 km horizontal resolution and 32 terrain following vertical layers and includes sea-ice dynamics, as well as mechanical and thermodynamic interaction between ice shelves and the ocean. The model time run spans seven years and simulates fourteen different tracers to understand dFe supply across the entire Antarctic coastal zone, with the last two years simulating biological uptake. For the purpose of this study, we only use four different dFe sources/tracers in the ASE: ice shelf melt, CDW, sediments and sea ice. Each tracer estimation is independent from each other, meaning that one source does not affect the other, and they have the same probability for biological uptake by phytoplankton. That is, dFe from all sources can equally be taken up by phytoplankton. This is parametrized in the model as all Fe molecules being bound to a ligand and therefore remaining in solution in a bioavailable form (Gledhill and Buck, 2012). For a detailed and complete explanation of the model, see Dinniman et al. (2020).

2.5 Other environmental parameters

We used SIC data spanning June 1998 to June 2017 from the National Snow and Ice Data Center (Cavalieri et al., 1996). The data are Nimbus-7 SMMR and SSMI/SSMIS passive microwave daily SIC with 25 km spatial resolution. We computed the sea-ice retreat time (IRT) and open water period (OWP) metrics using a 15 % threshold (Stammerjohn et al., 2008). Daily data were monthly averaged to perform a spatial correlation analysis (see Sect. 2.6).

We collected monthly level-4 Optimum Interpolation Sea Surface Temperature (OISST.v2) 0.25° high resolution dataset from the National Oceanic and Atmospheric Administration (Huang et al., 2021). Using this dataset compared to others has been proven to be the most suitable for our region of interest (Yu et al., 2023).

We obtained monthly Photosynthetically Available Radiation (PAR) from the same Globcolour project at the same spatial and temporal resolution (0.04° and 8 d) as chl *a*.

We used monthly averaged ERA5 reanalysis of zonal (*u*) and meridional (*v*) surface wind speed at 10 m above the surface (Hersbach et al., 2020).

We investigated monthly mean MLD from the Estimating the Circulation and Climate of the Ocean (ECCO) ocean and sea-ice state estimate project (ECCO consortium et al., 2021). The dataset is the version 4, release 4, at 0.5° spatial resolution.

Variability in the sea-ice landscape can be influenced by the Amundsen Sea Low (ASL) in West Antarctica (Hosking et al., 2013; Turner et al., 2016). We therefore finally looked at the impact of the ASL and its potential influence on sea-ice variability. Monthly ASL indices (latitude, longitude, central and sector pressure) derived from ERA5 reanalysis data were obtained from the ASL climate index page (Hosking et al., 2016).

2.6 Statistical analysis

Because some of our data were not normally distributed, we consistently applied nonparametric tests throughout our statistical analysis. A Mann-Kendall test was performed to detect linear trends in chl *a* and NPP. A two-tailed nonparametric Spearman correlation metric (*rho*, *p*) was calculated to investigate the relationship between chl *a*, NPP, and environmental factors, as well as between the phytoplankton bloom and sea-ice phenology metrics. A two-tailed Mann-Whitney test was performed to detect any significant mean differences for chl *a*, sea-ice phenology metrics, MLD, PAR and dFe sources between the two polynyas. Monthly spatial correlations were tested between SIC, winds, chl *a*, NPP, SST, and PAR after removing the seasonality for each parameter. As well, a yearly spatial correlation between chl *a*, NPP and TVFall was performed. The relationships between chl *a*, NPP and environmental factors were explored using a Principal Component Analysis (PCA). No pre-treatment (mean-centering or normalization) was applied to the variables prior to PCA, as all variables are expressed in comparable units and ranges, consistent with common practice in marine biogeochemistry studies (Marchese et al., 2017; Liniger et al., 2020). The Spearman, Mann-Whitney and PCA analysis were conducted using the mean TVFs, MLD, SST, and PAR calculated over the October-March period for each year, with the associated bloom and sea-ice phenology metrics. Every statistical test was run with a 95 % (*p*-value < 0.05) confidence level. Our study spans 1998–2017. We are constrained by the start of satellite ocean color data (1998) and the end of the ice shelf basal melt rate record (2017) from Paolo et al. (2023).

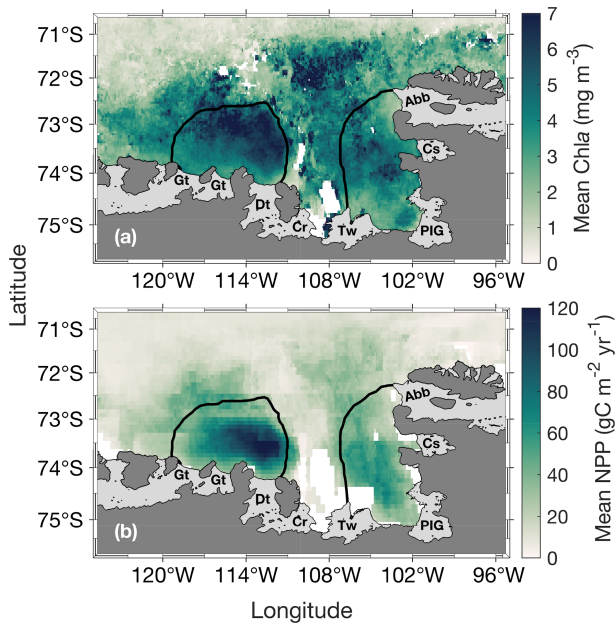


Figure 2. Spatial distribution of (a) mean surface chlorophyll-*a* (chl *a*) concentration during the bloom and (b) net primary productivity (NPP) climatology (1998–2017) for the Amundsen (ASP; left) and Pine Island (PIP; right) polynyas. The black lines represent the climatological summer polynyas' boundaries.

3 Results

3.1 Glacial meltwater, chl *a*, and NPP variability

The annual climatology maps reveal substantially higher chl *a* and NPP in the ASP compared to the PIP (Fig. 2). Chla starts increasing in mid-November to reach its average peak earlier in the PIP than the ASP. At its peak, chl *a* in the ASP is $6.49 \pm 1.29 \text{ mg m}^{-3}$ and $4.94 \pm 1.11 \text{ mg m}^{-3}$ in the PIP (Fig. 3a). During the bloom period, chl *a* is also higher in the ASP on average compared to the PIP ($\text{ASP} = 5.21 \pm 1.29 \text{ mg m}^{-3}$; $\text{PIP} = 3.69 \pm 1.11 \text{ mg m}^{-3}$; p -value < 0.01 ; Fig. 3b; Table S1). When looking at polynya area integrated values (concentration multiplied by area gives units of mg m^{-1}), chl *a* is significantly higher in the ASP than in the PIP, and increases with the polynya area (Figs. S1, S2). NPP is also significantly higher in the ASP than in the PIP ($1.88 \pm 1.12 \text{ TgC yr}^{-1}$ vs. $0.85 \pm 0.86 \text{ TgC yr}^{-1}$, p -value = 0.004; Fig. S3). No significant interannual trends in mean chl *a* and NPP during the bloom are observed for either polynya (p -value > 0.1 ; Figs. 3b, S3). The climatological winter MLD in the ASP is deeper (MLD ASP = $45.8 \pm 8.0 \text{ m}$; MLD PIP = $36.4 \pm 7.3 \text{ m}$; p -value < 0.01 ; Fig. 1b), indicating that it may better entrain deeper sources of nutrients into the upper waters for the following phytoplankton growing season, resulting in higher productivity (Fig. 2).

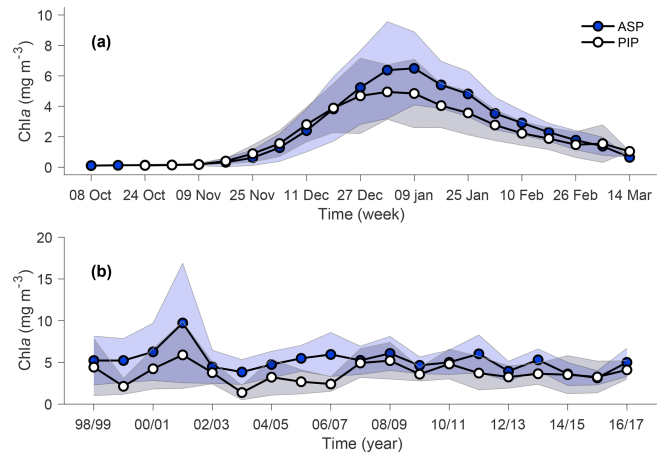


Figure 3. (a) Weekly chlorophyll-*a* (chl *a*) concentration climatology (1998–2017) for the Amundsen (ASP; blue circles) and Pine Island (PIP; white circles) polynyas. (b) Bloom mean chl *a* time series of ASP (blue circles) and PIP (white circles). Shaded areas represent the standard deviation for a given year. The relationship between chl *a* (in mg m^{-3} and mg m^{-1}) and the polynya size is shown in Fig. S2.

The variability in TVFall is statistically uncorrelated with surface chl *a* and NPP in both polynyas from 1998 to 2017 (Figs. 4, S4). However, the relationship becomes strongly significant in the ASP for both mean and maximum chl *a* when we remove the chl *a* outlier in 2001/02 (red data point; Fig. 4a–b), although not for NPP (Fig. S4a–b). The positive relationship implies that surface chl *a* in the ASP is higher when more glacial meltwater is delivered to the embayment. No strong relationships are observed in the PIP between TVFall, surface chl *a* and NPP (Figs. 4c–d, S4c–d).

When fluxes from individual glaciers are considered, PIP chl *a* does not correlate with Abbot, Cosgrove, PIG, Thwaites or TVFpip fluxes (Table 1). On the other hand, ASP chl *a* shows strong relationships with TVFasp, the Dotson and Crosson ice shelves (Table 1), and all ice shelves become significantly correlated with mean and maximum chl *a* when year 2001/02 is removed. There are no statistically significant relationships between individual ice shelves and NPP in either polynyas.

Spatially, the mean and maximum chl *a* are strongly correlated with TVFall in southern-eastern part of the ASP, in front of the Dotson ice shelf (Fig. 5a–b), where a positive relationship with NPP is also observed (Fig. 5c), although not significant.

3.2 Simulated dFe sources distribution

The modelled spatial distribution of surface dFe sources is presented in Fig. 6. On average, the smallest dFe source in the embayment is from ice shelves, with a maximum concentration between the Thwaites and Dotson ice shelves. The dFe from sea ice is slightly higher than from ice shelves and

Table 1. Statistical summary (Spearman's rank correlation) of the relationships between ice shelves volume flux, mean and maximum (max) surface chlorophyll-*a* (chl *a*) concentrations ($n = 19$) in both polynyas. The * marks a significant (p -value < 0.05) relationship. All relationships between mean chl *a*, maximum chl *a* and ASP ice shelves become significant when year 2001/02 is removed.

	Amundsen Sea polynya (ASP)				Pine Island polynya (PIP)			
	Mean chl <i>a</i>		Max chl <i>a</i>		Mean chl <i>a</i>		Max chl <i>a</i>	
	rho	<i>p</i> -value	rho	<i>p</i> -value	rho	<i>p</i> -value	rho	<i>p</i> -value
Abbot	/	/	/	/	0.09	0.73	-0.04	0.88
Cosgrove	/	/	/	/	-0.32	0.18	-0.46	0.05
PIG	/	/	/	/	-0.04	0.88	-0.13	0.61
Thwaites	0.16	0.52	0.11	0.66	0.12	0.63	0.09	0.71
Crosson	0.43	0.07	0.50	0.03*	/	/	/	/
Dotson	0.48	0.04*	0.54	0.02*	/	/	/	/
Getz	0.37	0.12	0.43	0.07	/	/	/	/
TVFasp	0.42	0.07	0.46	0.05*	/	/	/	/
TVFpip	/	/	/	/	0.009	0.97	-0.1	0.68

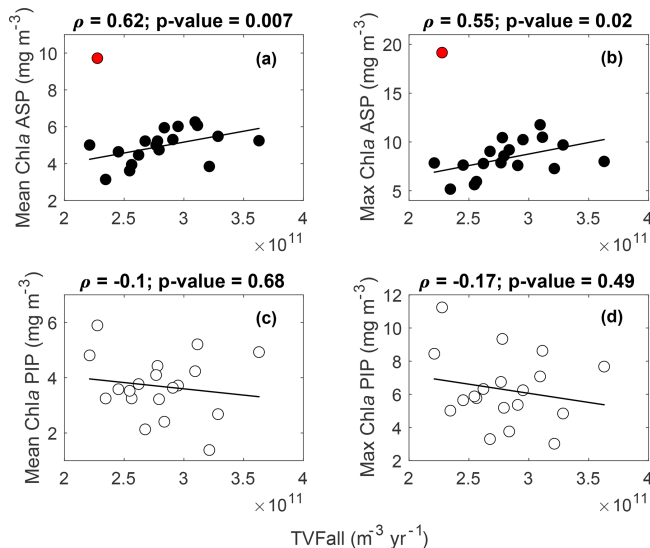


Figure 4. Scatter plots of mean and maximum (max) surface chlorophyll-*a* (chl *a*) concentrations with the total volume flux (TVFall) for the Amundsen (ASP) (a–b) and the Pine Island (PIP) (c–d) polynyas from 1998 to 2017 ($n = 19$). The fitted lines and statistics exclude year 2001/02 (red outlier) for the ASP regressions. If all data are considered, the relationships between mean chl *a*, max chl *a* and TVFall in the ASP are not significant. TVFall is an annual integral representing the sum of all ice shelves (see methods section) for the Amundsen Sea Embayment (ASE).

similar over the two polynyas, and is higher near the sea-ice margin (Fig. 6b). The dFe from CDW is also higher between the Thwaites and Dotson (Fig. 6c). Sediment is the dominant dFe source (Fig. 6d). Its distribution spreads from 108° W to the western part of the Getz ice shelf. The highest sediment-sourced dFe concentration is found along the coast and inside the ASP. On polynya-wide average basis, the sediment reservoir contributes significantly more to to-

tal dFe in the ASP (58.3 %, 0.13 nM) compared to sea ice (16.5 %, 0.04 nM), CDW (13.5 %, 0.03 nM) and ice shelves (11.7 %, 0.03 nM). In the PIP, the contribution of sediments is still significantly higher (41.2 %; 0.08 nM) but lower than the ASP and the contribution gap with the other sources decreases. The CDW and sea ice contribute 22.5 % (0.04 nM) and 18.9 % (0.035 nM) to the dFe pool respectively, while ice shelves are still the smallest sources at 14.5 % (0.03 nM) in the PIP.

3.3 Environmental parameters, chl *a* and NPP variability

During the phytoplankton growth season (October–March), SIC is spatially significantly anticorrelated to the meridional winds speed in both polynyas (Fig. 7a). Chl *a* is significantly positively correlated with SST in the eastern ASP, and the whole PIP (Fig. 7b), but weakly with PAR in both polynyas (Fig. 7c). Finally, PAR and SST are positively related in both central polynyas, albeit not significantly (Fig. 7d). We note that similar spatial relationships are observed when NPP is correlated with SST and PAR (Fig. S5).

Regarding the phenology, the bloom start is positively correlated to IRT and negatively with OWP in the ASP, although not significantly with the OWP (Table 2). This means that the bloom starts earlier and later as IRT does, and that longer OWP and earlier bloom starts are correlated with earlier ice retreat. The bloom mean and bloom maximum (max) chl *a* are not correlated with either IRT and OWP in the ASP. IRT and OWP are significantly related ($p = -0.93$; p -value < 0.001). When year 2001/02 is removed, no significant changes in the relationships between all parameters are detected. In the PIP, all metrics are significantly related to each other, except for PAR and OWP (Table 2). That is, the bloom start is positively correlated with IRT and negatively with OWP, while the bloom duration, mean chl *a*, max chl *a*

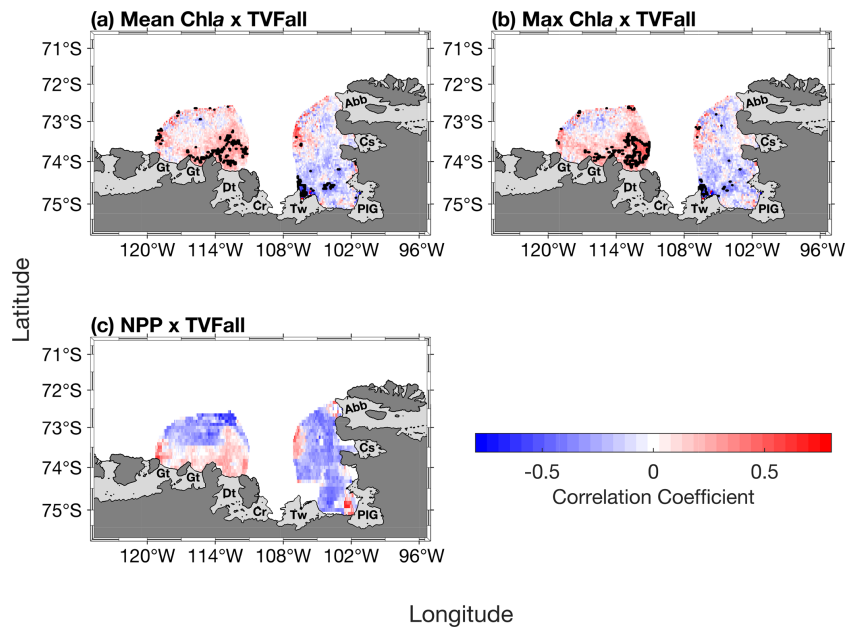


Figure 5. Spatial correlation maps between total volume flux (TVFall) and (a) surface mean chlorophyll-*a* (chl *a*) concentration, (b) surface maximum (max) chl *a* concentration and (c) net primary productivity (NPP) ($n = 19$). The black contour represents significant correlations at 95 % confidence level. Data outside of the summer climatological polynyas' boundaries were masked out.

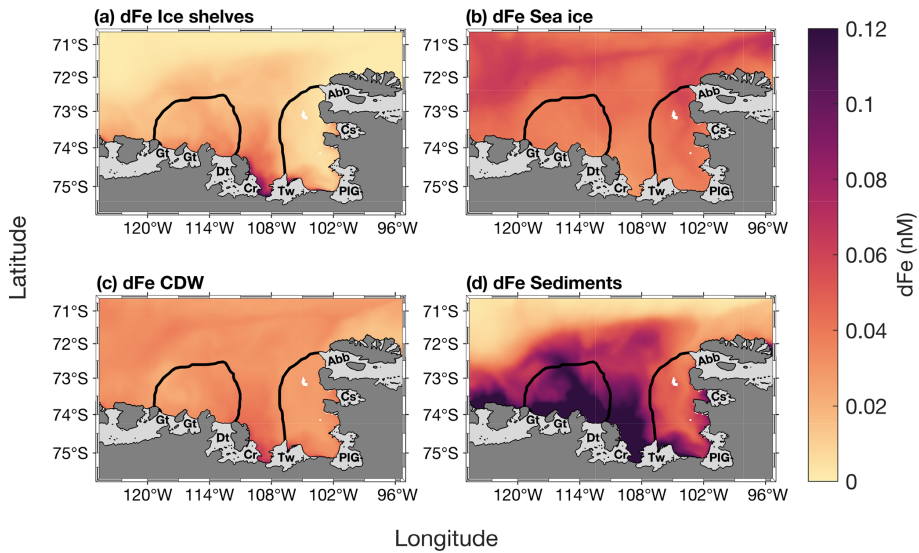


Figure 6. Two-years top-100 m averaged spatial distribution of surface dissolved iron (dFe) contribution from (a) ice shelves, (b) sea ice, (c) circumpolar deep water (CDW) and (d) sediments simulated by the model from Dinniman et al. (2020). The black lines represent the climatological summer polynya boundaries.

and NPP are negatively linked to the IRT and positively with OWP. SST and PAR are negatively correlated with IRT, and positively with OWP. IRT and OWP are significantly related in the PIP ($p = -0.88$; p -value < 0.001).

We explore the relationships between phytoplankton bloom phenology metrics and their potential environmental drivers by conducting a multivariate PCA for both polynyas (Fig. 8). The PCA reduces our datasets (11 variables) and

breaks them down into dimensions that capture most of the variability and relationships between all variables. Arrows indicate the contribution of each variable to the dimensions, with longer arrows representing stronger influence. Observations (in our case, years) positioned in the direction of an arrow are more influenced by that variable. In the ASP (Fig. 8a), the first two principal components explain 55.3 % of the total variance (Dim1: 35 %, Dim2: 20.3 %). NPP in

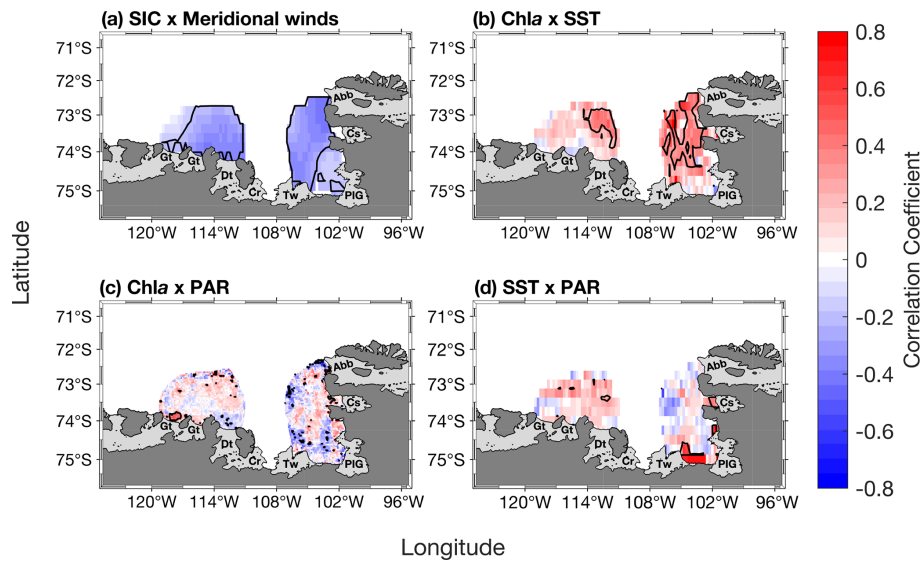


Figure 7. (a) Spatial correlation map between sea-ice concentration (SIC) and meridional winds. Spatial correlation maps between mean chlorophyll-*a* (chl *a*) concentration and (b) sea surface temperature (SST), (c) photosynthetically available radiation (PAR). (d) Spatial correlation map between PAR and SST. Data span 1998–2017 from October to March ($n = 114$). The black contour represents significant correlations at 95 % confidence level. Seasonality was removed before performing the correlation. Data outside of the summer climatological polynyas' boundaries were masked out.

Table 2. Statistical summary (Spearman's rank correlation) of the relationships between the sea-ice phenology metrics and environmental parameters ($n = 19$) in both polynyas. The * marks a significant (p -value < 0.05) relationship. IRT = ice retreat time, OWP = open water period, NPP = net primary productivity, SST = sea surface temperature, PAR = photosynthetically available radiation. Removing year 2001/02 for the ASP slightly changes the strength of the relationships between parameters (i.e., rho) but not the significance.

	Amundsen Sea polynya (ASP)				Pine Island polynya (PIP)			
	IRT		OWP		IRT		OWP	
	rho	<i>p</i> -value	rho	<i>p</i> -value	rho	<i>p</i> -value	rho	<i>p</i> -value
Bloom start	0.51	0.03*	-0.43	0.07	0.56	0.02*	-0.48	0.04*
Bloom duration	-0.12	0.63	0.09	0.71	-0.56	0.02*	0.59	0.01*
Bloom mean	0.19	0.44	-0.33	0.17	-0.67	0.003*	0.50	0.04*
Bloom max	0.24	0.32	-0.35	0.14	-0.65	0.005*	0.52	0.03*
NPP	-0.55	0.02*	0.45	0.05	-0.72	0.001*	0.54	0.02*
SST	-0.09	0.72	-0.01	0.96	-0.57	0.02*	0.52	0.03*
PAR	-0.09	0.72	0.05	0.84	-0.62	0.007*	0.38	0.12

the ASP is closely associated with BD, indicating that the bloom duration is the primary driver of production. On the other hand, environmental vectors such as TVFall and TV-Fasp project more strongly onto Dim2 with the bloom mean chl *a*, indicating that meltwater input may influence surface chl *a* interannual variability, and is less directly tied to NPP. We note that when year 2001/02 is removed, the relationship between TVFasp and TVFall becomes much stronger with BM (Fig. S6a) and is slightly anticorrelated to SST and MLD. In the PIP (Fig. 8b), the first two components account for 63.7 % of the total variance (Dim1: 46.7 %, Dim2: 17 %). Compared to the ASP, both NPP and BM cluster strongly with BD and PAR on Dim1. Additionally, IRT, OWP and

SST and MLD aligned along Dim1, which explains 46.7 % of the total variance compared to 35 % for the ASP, suggesting that physical conditions might play a stronger structuring role in PIP compared to the ASP. In contrast, TVFall and TVF-PIP stand alone and align more strongly with Dim2, suggesting a less dominant influence of meltwater on BM and NPP variability in the PIP. The summer polynya-averaged PAR and MLD are significantly stronger and deeper, respectively, in the ASP compared to the PIP during the bloom season (MLD ASP = 28.5 ± 5.7 m; MLD PIP = 24.9 ± 3.7 m; p -value = 0.03 and PAR ASP = 31.5 ± 5.4 Einstein $m^{-2} d^{-1}$; PAR PIP = 26.5 ± 6.7 Einstein $m^{-2} d^{-1}$; p -value = 0.02).

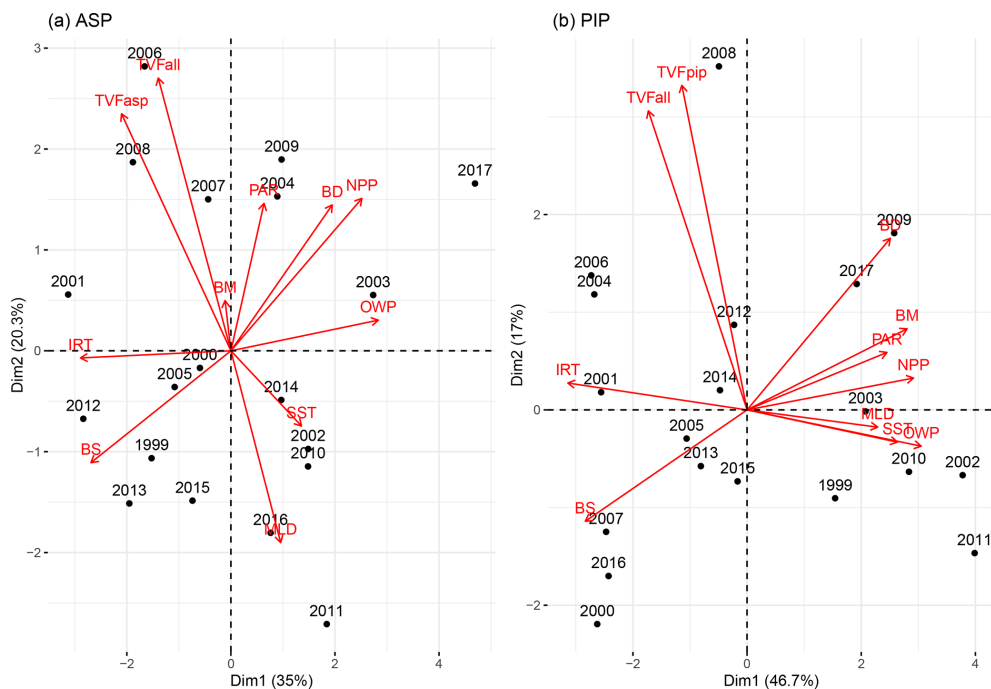


Figure 8. Principal component analysis biplot of environmental parameters (red) and years (black) for (a) the Amundsen (ASP) and (b) the Pine Island (PIP) polynyas. TVFasp = total volume flux for ASP; TVFpip = total volume flux for PIP; TVFall = total volume flux for all ice shelves; BM = bloom mean; PAR = photosynthetically available radiation; BD = bloom duration; NPP = net primary productivity; OWP = open water period; SST = sea surface temperature; MLD = mixed-layer depth; BS = bloom start; IRT = ice retreat time. The same plot is presented in Fig. S6, but removing year 2001/02 for the ASP, emphasizing the relationship between total volume flux (TVFall, TVFasp) and BM in the ASP.

Finally, we find on average weak spatial negative relationships between SIC and ASL latitude, longitude, mean sector and actual central pressure in both polynyas during the growing season (Fig. S7), and only slightly significant in the eastern PIP.

4 Discussion

4.1 Effect of glacial meltwater on phytoplankton chl *a* and NPP

The relationship between glacial meltwater, surface chl *a* and NPP observed over the last two decades was distinctly different between the two polynyas. In the ASP, we found that enhanced glacial meltwater translates into higher surface chl *a*, but not with NPP (when removing year 2001/02; Figs. 4a–b, S6a). Modelling results (Fig. 6) suggest that sediment from the seafloor is the main source of dFe in the ASP, but this source is also linked to glacial melt. Ice shelf glacial meltwater drives the meltwater pump, which brings up mCDW and fine-grained subglacial sediments to the surface. This result is in agreement with previous research: Melt-laden modified CDW flowing offshore from the Dotson ice shelf to the central ASP (Sherrell et al., 2015), and resuspended sediments (Dinniman et al., 2020; St-Laurent et al., 2017, 2019).

have been identified as significant sources of dFe to be used by phytoplankton. Interestingly, both dFe supplied from ice shelves and CDW are most important in front of the Thwaites and Crosson ice shelves, where the area averaged basal melt rate, and thus likely the area averaged meltwater pumping (Jourdain et al., 2017), are typically strongest in observations (Adusumilli et al., 2020; Rignot et al., 2013) and modelling (Fig. 6). The year 2001/02 does not stand out as being influenced by any specific parameter in the ASP compared to other years (Figs. 8a, S6a). The anomalously high surface chl *a* observed during this year, as also reported by Arrigo et al. (2012), may result from exceptional conditions that were not captured by the parameters analysed in our study, for instance, an imbalance in the grazing pressure. Interestingly, surface chl *a* and NPP exhibit contrasting trends when averaged across the polynya. While TVFall may explain some of the variance in surface chl *a*, it does not account for the variance in NPP, whether assessed through direct or multivariate relationships. This decoupling between chl *a* and NPP in the ASP suggests that glacial meltwater, while enhancing surface phytoplankton biomass through nutrient delivery, may also promote vertical mixing. This mixing deepens the mixed layer, reducing light availability and constraining photosynthetic rates. These rates are influenced by fluctuations in the MLD, even in the presence of high biomass and suf-

ficient macronutrients. The summer MLD is deeper in the ASP, which would decrease light availability, despite higher PAR compared to the PIP. Previous studies report that the small prymnesiophyte *P. antarctica*, a low-efficiency primary producer (Lee et al., 2017), is better adapted to deeper mixed layers and therefore lower light conditions (Alderkamp et al., 2012; Mills et al., 2010) and could contribute to high surface chl *a* decoupled from NPP, as observed in the ASP. This is consistent with past in situ studies showing systematic differences in mixed-layer structure between the two polynyas. The PIP commonly exhibits a shallow, strongly stratified surface mixed layer while the ASP is more variable and has been observed to host deeper MLD (Alderkamp et al., 2012; Park et al., 2017; Yager et al., 2016; Mills et al., 2012). Near glacier and ice-shelf fronts, entrainment of 'Fe-rich deep waters rising to the surface through the meltwater pump can also produce surface chl *a* maxima (high biomass from *P. antarctica*) without proportional increases in depth-integrated productivity due to self-shading (Twelves et al., 2021). Further from the coast, meltwater spreading at neutral buoyancy strengthens stratification, limiting vertical nutrient fluxes and thereby suppressing NPP despite elevated chl *a*. These dual mechanisms are consistent with observational and modelling studies of meltwater entrainment and dispersal (Randall-Goodwin et al., 2015; St-Laurent et al., 2017; Dinniman et al., 2020; Forsch et al., 2021), and suggest that spatial heterogeneity in plume dynamics could explain the observed chl *a* and NPP mismatch.

In the PIP, we did not find any long-term relationships between the phytoplankton bloom, NPP and glacial meltwater. Variability in ice shelf glacial meltwater may not have the same effect on the surface chl *a* and NPP in the PIP compared to the ASP. Iron delivered from glacial melt process related in the PIP and west of it could accumulate and follow the westward coastal current, towards the ASP (St-Laurent et al., 2017). These sources would include dFe from meltwater pumped CDW, sediments and ice shelves, all of which are higher in front of the Crosson ice shelf, west of the PIP (Fig. 6). With the coastal circulation, this would make dFe supplied by glacial meltwater greater in the ASP, thereby contributing to the higher productivity in the ASP. Recently, subglacial discharge (SGD) was shown to have a different impact on basal melt rate in the ASE polynyas (Goldberg et al., 2023), where PIG had a lot less relative increase in melt with SGD input than Thwaites or Dotson/Crosson. Thus, assuming a direct relationship between meltrate, SGD and dFe sources, the signal in the PIP (fed by PIG melt) will be much weaker than in the ASP (fed by upstream Thwaites, Crosson and local Dotson due to the circulation), which might also explain the discrepancies between the PIP and ASP. A stronger meltwater-driven stratification may also dominate in the PIP, reducing vertical nutrient replenishment and thereby limiting biomass growth (Oh et al., 2022), even where TVFall is high, hence leading to a direct negative relationship observed compared to the ASP (Figs. 4, S4). The model outputs used here

are critical to understand the spatial distribution of dFe in the embayment. They strongly suggest, but do not definitively demonstrate, the role of dFe in influencing the phytoplankton bloom interannual variability.

Satellite algorithms commonly estimate NPP from surface chl *a*, but the approach and assumptions vary across models. The VGPM relates chl *a* to depth-integrated photosynthesis through empirical relationships with light and temperature (Behrenfeld and Falkowski, 1997). In contrast, the Carbon-based Productivity Model (CbPM) emphasizes phytoplankton carbon biomass and growth rates derived from satellite optical properties, decoupling productivity estimates from chl *a* alone (Westberry et al., 2008). The CAFE model (Carbon, Absorption, and Fluorescence Euphotic-resolving model) integrates additional physiological parameters such as chl *a* fluorescence and absorption to better constrain phytoplankton carbon fixation (Silsbe et al., 2016). In the Southern Ocean, where light limitation, Fe supply, and community composition strongly influence the relationship between chl *a* and productivity, these algorithmic differences can yield substantial variability in NPP estimates (Ryan-Keogh et al., 2023), with studies showing that VGPM-type models often outperform CbPM in coastal Southern Ocean regions (Jena and Pillai, 2020). Because the VGPM algorithm does not explicitly incorporate the MLD, but instead estimates primary production integrated over the euphotic zone based on surface chl *a*, PAR, and temperature, it may not fully capture the influence of variable MLD or subsurface processes related to glacial melt, which could contribute to the observed decoupling between chl *a* and NPP. Therefore, while the observed decoupling between chl *a* and NPP in the ASP might also come from our choice of dataset, the VGPM model may be more appropriate for coastal polynya environments, such as those in the Amundsen Sea. We finally note as a limitation that satellite-derived chl *a* and VGPM NPP estimates lack the vertical resolution needed to resolve sub-plume stratification and mixing processes (e.g., fine-scale vertical gradients in Fe or nutrient fluxes), so our mechanistic interpretations of surface chl *a* vs. depth-integrated productivity decoupling must be taken with caution.

Direct observations from Sherrell et al. (2015) showed higher chl *a* in the central ASP while surface dFe was low weeks before the bloom peak. This suggests a continuous supply and consumption of dFe in the area, most likely from the circulation, as mentioned earlier. Considering the long residence time of water masses in both polynyas (about 2 years (Tamsitt et al., 2021)), and the daily dFe uptake by phytoplankton ($3\text{--}196 \text{ pmol L}^{-1} \text{ d}^{-1}$ (Lannuzel et al., 2023)), we also hypothesise that any dFe reaching the upper ocean from external sources is quickly used and unlikely to remain readily available for phytoplankton in the following spring season.

In recent model simulations with the meltwater pump turned off, Fe becomes the principal factor limiting phytoplankton growth in the ASP (Oliver et al., 2019). However,

the transport of Fe-rich glacial meltwater outside the ice shelf cavities and to the ocean surface depends strongly on the local hydrography. While Garabato et al. (2017) suggested that the glacial meltwater concentration and settling depth (neutral buoyancy) outside the ice shelf cavities is controlled by an overturning circulation driven by instability, others suggest that the strong stratification plays an important role in how close to the surface the buoyant plume of said meltwater can rise (Arnscheidt et al., 2021; Zheng et al., 2021). Therefore, high melting years and greater TVFall might not necessarily translate into a more Fe-enriched meltwater delivered to the surface outside the ice shelf cavities, close to the ice shelf edge, as rising water masses may be either prevented from doing so, or be transported further offshore in the polynyas where the phytoplankton bloom occurs, before they can resurface (Herraiz-Borreguero et al., 2016).

Although several Fe sources can fuel polynya blooms, and they depend on processes mentioned above, Fe-binding ligands may ultimately set the limit on how much of this dFe stays dissolved in the surface waters (Gledhill and Buck, 2012; Hassler et al., 2019; Tagliabue et al., 2019). Models of the Amundsen Sea (Dinniman et al., 2020, 2023; St-Laurent et al., 2017, 2019) did not include Fe complexation with ligands and assumed a continuous supply of available dFe for phytoplankton. Spatial and seasonal data on Fe-binding ligands along the Antarctic coast remain extremely scarce and their dynamics are poorly understood (see Smith et al. (2022) for a database of publicly available Fe-binding ligand surveys performed south of 50° S). Field observations in the ASP and PIP suggest that the ligands measured in the upwelling region in front of the ice shelves had little capacity to complex any additional Fe supplied from glacial melt. As a consequence, much of the glacial and sedimentary Fe supply in front of the ice shelves could be lost via particle scavenging and precipitation (Thuróczy et al., 2012). This was also observed by van Manen et al. (2022) in the ASP. However, within the polynya blooms, Thuróczy et al. (2012) found that the ligands produced by biological activity were capable of stabilising additional Fe supplied from glacial melt, where we observed the highest productivity. The production of ligands by phytoplankton would increase the stock of bioavailable dFe and further fuel the phytoplankton bloom in the polynyas, potentially highlighting the dominance of *P. antarctica*, which uses Fe-binding ligands more efficiently than diatoms (Thuróczy et al., 2012), even under low light conditions. Model development and sustained field observations on dFe availability, including ligands, are needed to adequately predict how these may impact biological productivity under changing glacial and oceanic conditions, now and in the future.

Overall, the discrepancies observed between the ASP and PIP point to a complex set of ice-ocean-sediment interactions, where several co-occurring processes and differences in hydrographic properties of the water column influence dFe supply and consequent primary productivity.

4.2 Possible drivers of the difference in phytoplankton surface chl *a* and NPP between the two polynyas

The biological productivity is higher in the ASP than the PIP, consistent with previous studies (Arrigo et al., 2012; Park et al., 2017). In Sect. 4.1, we mentioned the suspected underlying hydrographic drivers of these differences. We related the higher biological productivity in the ASP to a potentially greater supply of Fe from melt-laden dFe-enriched mCDW and sediment sources, but this difference in productivity could also be attributed to other local features. The Bear Ridge grounded icebergs on the ASP's eastern side (Bett et al., 2020) could add to the overall meltwater pump strength. They can enhance warm CDW intrusions to the ice shelf cavity (Bett et al., 2020), increasing ice shelf melting and subsequent stronger phytoplankton bloom from the meltwater pump activity. These processes are weaker or absent in the PIP. Few sources other than glacial meltwater may influence the bloom in the PIP. For instance, dFe in the euphotic zone can also be sustained by the biological recycling, as shown in the PIP by Gerringa et al. (2020).

Sea ice could also partly explain the difference in chl *a* magnitudes, NPP, and variability between the ASP and PIP. The strong spatial correlation between SIC and meridional winds (Fig. 7a) indicates that southerly winds can export the coastal sea ice offshore and play a significant role in opening the polynyas. In the ASP compared to the PIP, sea ice retreats earlier (IRT = 1 January \pm 14 d vs. 18 January \pm 17 d, *p*-value = 0.003), the open water period is longer (OWP = 61 \pm 16 d vs. 44 \pm 22 d, *p*-value < 0.001), and the SIC is lower (Fig. S8). In the ASP, an early sea-ice retreat leads to an earlier bloom start, but the longer open water period is not significantly associated with greater bloom mean or maximum chl *a* (Table 2). On the other hand in the PIP, an early sea-ice retreat also triggers an early bloom start, but the longer open duration is associated with warmer water, higher bloom mean chl *a*, maximum chl *a*, and NPP. These results suggest that different processes might drive phytoplankton growth variability in the two polynyas. In the ASP, it is likely the replenishment of dFe that mostly influences the bloom. In the PIP, higher SIC can delay the retreat time and shorten the open water season (Table 2, Fig. S8), leading to lower chl *a* and NPP compared to the ASP. The significant negative relationships between IRT, PAR, chl *a* and NPP in the PIP (Table 2, Fig. S6) suggests a strong light limitation relief in the polynya. This light limitation hypothesis is further supported by the high correlation between polynya-averaged chl *a* mean with PAR and SST in the PIP across the 19 years of study, compared to the lack of correlation in the ASP (Table S2; *p*-value < 0.01 for all relationships in the PIP). While *P. antarctica* is usually the main phytoplankton species dominating in both polynyas, the combination of light-limitation relief and higher SST may create better conditions for a stratified and warmer environment that would favor diatom (Arrigo et al., 1999; van Leeuwe et al., 2020), as recently ob-

served in the ASP (Lee et al., 2022). The positive association of PAR, SST and chl *a* with MLD likely reflects conditions around sea-ice retreat (all negatively associated with IRT), when enhanced wind mixing deepens the mixed layer and replenishes surface nutrients while light availability and SST increases. This nutrient-light co-limitation phase supports high biomass accumulation, likely from diatoms. Similar results have been reported by Park et al. (2017). They found that the PIP was not limited by dFe, potentially from biological recycling (Gerringa et al., 2020), compared to an Fe-limited ASP. We hypothesise that the connection between glacial meltwater and chl *a* that we found in the ASP is a response to Fe input (also observed by Park et al. (2017) during incubation experiments) compared to the PIP, where light and temperature seem to play a more significant role in driving the phytoplankton bloom variability. Hayward et al. (2025) showed a decline in diatoms from 1997 to 2017 in the PIP. However, they observed an increase in diatoms after 2017, linked to regime shift in sea ice. Their study also indicates that diatoms are competitively disadvantaged under Fe-depleted conditions. *P. antarctica*, which relies on dFe supplied by ocean circulation, would then tend to dominate in the ASP. Such shifts in phytoplankton composition are likely to affect carbon export, grazing, and higher trophic levels. Additional long-term data on inter-annual variability in phytoplankton composition and physiology will be essential to fully understand these relationships.

Finally, the weak relationships between the ASL indices and SIC might be owing to the seasonal variation of the ASL, where its position largely varies during summer, and its impact in shaping coastal sea ice is also greater during winter and autumn in the Amundsen-Bellingshausen region (Hosking et al., 2013). The lack of strong significant relationships overall does not allow us to conclude that the ASL plays an important role in shaping the coastal polynyas landscape and influencing chl *a* variability.

4.3 Limitations and future directions

We acknowledge that elevated concentrations of suspended sediments (and non-photosynthetically active particles in general) near the ocean surface can impart optical signatures that bias satellite-derived chl *a* high in coastal waters. Consequently, the higher chl *a* observed in the ASP relative to the PIP, as well as the weak correspondence between chl *a* and NPP in ASP, may reflect some sediment-driven optical effects rather than enhanced phytoplankton biomass or productivity alone. While our results are consistent with known differences in Fe supply and mixed-layer dynamics between the two polynyas, the potential contribution of sediment-related bias cannot be ruled out and should be acknowledged when interpreting spatial contrasts in satellite chl *a* on the Antarctic shelf.

While it seems reasonable that the higher ASP productivity could be driven by more Fe delivered through a stronger meltwater pump downstream of the PIP, our data cannot confirm this hypothesis. To accurately understand the role of Fe through the meltwater pump process, we would need to quantify the fraction of meltwater and glacial modified water (mix of CDW and ice shelf meltwater) reaching the ocean surface, together with the Fe content. Obtaining this information is challenging over the decadal time scales considered and the method used in our study. Here, our intention was to provide valuable insights into the potential drivers of our results, and highlight the benefit of remote sensing, in this poorly observed environment. Our work directly aligns with Pan et al. (2025), who investigated the long-term relationship between sea surface glacial meltwater and satellite surface chl *a* in the Western Antarctic Peninsula, and found a strong relationship between the two parameters, highlighting the importance of glacial meltwater discharge in regions prone to extreme and rapid climate changes.

In multimodel climate change simulations, Naughten et al. (2018) showed an increase of ice shelves melting up to 90 % on average, attributed to more warm CDW on the shelf, due to atmospherically driven changes in local sea-ice formation. More recently, Dinniman et al. (2023) also highlighted the impact of projected atmospheric changes on Antarctic ice sheet melt. They showed that strengthening winds, increasing precipitation and warmer atmospheric temperatures will increase heat advection onto the continental shelf, ultimately increasing basal melt rate by 83 % by 2100. Compared to present climate simulations, their simulation showed a 62 % increase in total dFe supply to shelf surface waters, while basal melt driven overturning Fe supply increased by 48 %. The ice shelf melt and overturning contributions varied spatially, increasing in the Amundsen-Bellingshausen area and decreasing in East Antarctica. This implies that, under future climate change, phytoplankton productivity could show stronger spatial asymmetry around Antarctica. The increasing melting and thinning of ice shelves will eventually result in more numerous calving events and drifting icebergs (Liu et al., 2015). Model simulations stressed the importance of ice shelves and icebergs in delivering dFe to the SO (Death et al., 2014; Person et al., 2019), increasing offshore productivity. As Fe will likely be replenished and sufficient from increasing melting in coastal areas, it is possible that the system will shift from Fe-limited to being limited by nitrate, silicate, or even manganese (Anugerahanti and Tagliabue, 2024), while offshore SO productivity will likely remain Fe-dependent (Oh et al., 2022).

5 Conclusions

Using spatial and multivariate approaches, our study explored the variability of surface chl *a* and NPP in the Amundsen Sea polynyas over the last two decades, with a focus on

the main environmental characteristics of the ASE. We found a strong relationship between ice shelf melting and surface chl *a* in the ASP when year 2001/02 was removed, a result in agreement with the ASPIRE field studies and previous satellite analyses. On the other hand, we did not find clear evidence of such a relationship in the PIP, where light, sea surface temperature and open water availability seem more important. The differences between the polynyas may lie in hydrographic properties, or the use of satellite remote sensing itself, which cannot tell us about processes such as Fe supply, bioavailability and phytoplankton demand. To gain greater insight, we referred to model simulations that showed the spatial variability in the magnitude of iron sources. Our results call for sustained in situ observations (e.g., moorings equipped with trace-metal clean samplers, and physical sensors to better understand year-to-year water mass meltwater fraction and properties) to elucidate these long-term relationships. Satellite observations are a powerful tool to investigate the relationship between glacial meltwater and biological productivity on such time scales, which has until now relied almost exclusively on field observations and modelling. Using such tools, we showed how the relationship between phytoplankton and the environment varies spatially and temporally across 19 years.

Data availability. Bathymetry data (Amante and Eakins, 2009) was taken from the NOAA website (<http://www.ngdc.noaa.gov/mgg/global/global.html>, last access: 19 August 2025). Mixed-layer depth (ECCO Consortium et al., 2021) can be accessed here: https://podaac.jpl.nasa.gov/dataset/ECCO_L4_MIXED_LAYER_DEPTH_05DEG_MONTHLY_V4R4 (last access: 19 August 2025). Satellite surface chlorophyll-*a* and photosynthetically available radiation were downloaded from <https://www.globcolour.info/> (last access: 10 February 2025). Sea surface temperature (Huang et al., 2021) can be found here <https://psl.noaa.gov/data/gridded/data.noaa.oisst.v2.highres.html>. Wind re-analysis data (Hersbach et al., 2020) are available at <https://cds.climate.copernicus.eu/datasets/reanalysis-era5-single-levels-monthly-means?tab=download> (last access: 10 February 2025). Sea-ice concentration (Cavalieri et al., 1996) was obtained from <https://nsidc.org/data> (last access: 10 February 2025) and Net Primary productivity (Behrenfeld and Falkowski, 1997) was downloaded from <http://sites.science.oregonstate.edu/ocean.productivity/index.php> (last access: 10 February 2025). Circumpolar surface model output from Dinniman et al. (2020) can be found at <https://www.bco-dmo.org/dataset/782848> (last access: 10 February 2025). The Amundsen Sea Low index (Hosking et al., 2016) data are available at http://scotthosking.com/asl_index (last access: 10 February 2025).

Supplement. The supplement related to this article is available online at <https://doi.org/10.5194/bg-23-665-2026-supplement>.

Author contributions. GL conceptualised and led the study; MSD provided the dissolved iron model output. All authors were involved in the interpretation of the results, the revision, and the writing of the final version of the paper.

Competing interests. The contact author has declared that none of the authors has any competing interests.

Disclaimer. Publisher's note: Copernicus Publications remains neutral with regard to jurisdictional claims made in the text, published maps, institutional affiliations, or any other geographical representation in this paper. The authors bear the ultimate responsibility for providing appropriate place names. Views expressed in the text are those of the authors and do not necessarily reflect the views of the publisher.

Acknowledgements. We are grateful for the support of the University of Tasmania and the Australian Research Council (ARC) Centre of Excellence for Climate Extremes. We are also grateful to Will Hobbs, Rob Massom and Patricia Yager for their knowledgeable input. We thank Vincent Georges for some preliminary work as part of his masters' internship. We are very grateful to Fernando S. Paolo for his early input and help with the glacial meltwater dataset. We finally thank the data providers mentioned in the methods section for making their data available and free of charge.

Financial support. Guillaume Liniger was funded by the University of Tasmania and the ARC Centre of Excellence for Climate Extremes (grant no. CE17010002), and is currently funded by the Southern Ocean Carbon and Climate Observations and Modeling (SOCCOM) Project funded by the National Science Foundation, Division of Polar Programs (grant nos. NSF PLR-1425989 and OPP-1936222). Peter Strutton was funded by the Australian Research Council (ARC) Centre of Excellence for Climate Extremes (grant no. CE170100023), and currently by the Australian Centre for Excellence in Antarctic Science (ACEAS; grant no. SR200100008). Delphine Lannuzel is funded by the ARC through a Future Fellowship (grant no. L0026677). Sébastien Moreau received funding from the Research Council of Norway (RCN) for the project "I-CRYME: Impact of CRYosphere Melting on Southern Ocean Ecosystems and biogeochemical cycles" (grant no. 335512) and for the Norwegian Centre of Excellence "iC3: Center for ice, Cryosphere, Carbon and Climate" (grant no. 332635). Michael Dinniman was supported by the U.S National Science Foundation (grant no. OPP-1643652).

Review statement. This paper was edited by Yuan Shen and reviewed by three anonymous referees.

References

Adusumilli, S., Fricker, H. A., Medley, B., Padman, L., and Siegfried, M. R.: Interannual variations in meltwater input to the Southern Ocean from Antarctic ice shelves, *Nat. Geosci.*, 13, 616–620, <https://doi.org/10.1038/s41561-020-0616-z>, 2020.

Alderkamp, A.-C., Mills, M. M., van Dijken, G. L., Lann, P., Thuróczy, C.-E., Gerringa, L. J. A., de Barr, H. J. W., Payne, C. D., Visser, R. J. W., Buma, A. G. J., and Arrigo, K. R.: Iron from glaciers fuels phytoplankton blooms in the Amundsen Sea (Southern Ocean): Phytoplankton characteristics and productivity, *Deep-Sea Res. II*, 71–76, 32–48, <https://doi.org/10.1016/j.dsr2.2012.03.005>, 2012.

Amante, C. and Eakins, B. W.: ETOPO1 1 Arc-Minute Global Relief Model: Procedures, Data Sources and Analysis, NOAA Technical Memorandum NESDIS NGDC-24, NOAA National Geophysical Data Center [data set], <https://doi.org/10.7289/V5C8276M>, 2009.

Anugerahanti, P. and Tagliabue, A.: Response of Southern Ocean Resource Stress in a Changing Climate, *Geophys. Res. Lett.*, 51, e2023GL107870, <https://doi.org/10.1029/2023GL107870>, 2024.

Ardyna, M., Claustre, H., Sallée, J.-B., D’Ovidio, F., Gentili, B., van Dijken, G. L., D’Ortenzio, F., and Arrigo, K. R.: Delineating environmental control of phytoplankton biomass and phenology in the Southern Ocean, *Geophys. Res. Lett.*, 44, 5016–5024, <https://doi.org/10.1002/2016GL072428>, 2017.

Ardyna, M., Mundy, C. J., Mayot, N., Matthes, L. C., Oziel, L., Horvat, C., Leu, E., Assmy, P., Hill, V., Matrai, P. A., Gale, M., Melnikov, I. A., and Arrigo, K. R.: Under-Ice Phytoplankton Blooms: Shedding Light on the “Invisible” Part of Arctic Primary Production, *Front. Mar. Sci.*, 7, <https://doi.org/10.3389/fmars.2020.608032>, 2020.

Arnscheidt, C. W., Marshall, J., Dutrieux, P., Rye, C. D., and Ramadhan, A.: On the Settling Depth of Meltwater Escaping from beneath Antarctic Ice Shelves, *JPO*, 51, 2257–2270, <https://doi.org/10.1175/JPO-D-20-0286.1>, 2021.

Arrigo, K. R., Lowry, K. E., and van Dijken, G. L.: Annual changes in sea ice and phytoplankton in polynyas of the Amundsen Sea, Antarctica, *Deep-Sea Res. II*, 71–76, 5–15, <https://doi.org/10.1016/j.dsr2.2012.03.006>, 2012.

Arrigo, K. R., Robinson, D. H., Worthen, D. L., Dunbar, R. B., DiTullio, G. R., VanWoert, M., and Lizotte, M. P.: Phytoplankton community structure and the drawdown of nutrients and CO₂ in the Southern Ocean, *Science*, 283, 5400, 365–367, <https://doi.org/10.1126/science.283.5400.365>, 1999.

Arrigo, K. R. and van Dijken, G. L.: Phytoplankton dynamics within 37 Antarctic coastal polynya systems, *J. Geophys. Res. Ocean.*, 108, <https://doi.org/10.1029/2002JC001739>, 2003.

Arrigo, K. R., van Dijken, G. L., and Strong, A. L.: Environmental controls of marine productivity hot spots around Antarctica, *J. Geophys. Res. Ocean.*, 120, 5545–5565, <https://doi.org/10.1002/2015JC010888>, 2015.

Arrigo, K. R., Worthen, D., Schnell, A., and Lizotte, M. P.: Primary production in Southern Ocean waters, *J. Geophys. Res. Ocean.*, 103, 15587–15600, <https://doi.org/10.1029/98JC00930>, 1998.

Assmann, K. M., Jenkins, A., Shoosmith, D. R., Walker, D., Jacobs, S., and Nicholls, K.: Variability of circumpolar deep water transport onto the Amundsen Sea continental shelf through a shelf break trough, *J. Geophys. Res. Oceans*, 118, 6603–6620, <https://doi.org/10.1002/2013JC008871>, 2013.

Behrenfeld, M. J. and Falkowski, P. G.: Photosynthetic rates derived from satellite-based chlorophyll concentration, *Limnol. Oceanogr.*, 42, 1–20, <https://doi.org/10.4319/lo.1997.42.1.0001>, 1997.

Bett, D. T., Holland, P. R., Naveira Garabato, A. C., Jenkins, A., Dutrieux, P., Kimura, S., and Fleming, A.: The Impact of the Amundsen Sea Freshwater Balance on Ocean Melting of the West Antarctic Ice Sheet, *J. Geophys. Res. Oceans*, 125, <https://doi.org/10.1029/2020JC016305>, 2020.

Bhatia, M. P., Kujawinski, E. B., Das, S. B., Breier, C. F., Henderson, P. B., and Charette, M. A.: Greenland meltwater as a significant and potentially bioavailable source of iron to the ocean, *Nat. Geosci.*, 6, 274–278, <https://doi.org/10.1038/ngeo1746>, 2013.

Biddle, L. C., Heywood, K. J., Kaiser, J., and Jenkins, A.: Glacial Meltwater Identification in the Amundsen Sea, *JPO*, 47, 933–954, <https://doi.org/10.1175/JPO-D-16-0221.1>, 2017.

Boles, E., Provost, C., Garçon, V., Bertosio, C., Athanase, M., Koenig, Z., and Sennéchal, N.: Under-Ice Phytoplankton Blooms in the Central Arctic Ocean: Insights From the First Biogeochemical IAOOS Platform Drift in 2017, *J. Geophys. Res. Ocean.*, 125, e2019JC015608, <https://doi.org/10.1029/2019JC015608>, 2020.

Boyd, P. W., Jickells, T., Law, C. S., Blain, S., Boyle, E. A., Bueseler, K. O., Coale, K. H., Cullen, J. J., Baar, H. J. W. de, Follows, M., Harvey, M., Lancelot, C., Levasseur, M., Owens, N. P. J., Pollard, R., Rivkin, R. B., Sarmiento, J., Schaeemann, V., Smetacek, V., Takeda, S., Tsuda, A., Turner, S., and Watson, A. J.: Mesoscale Iron Enrichment Experiments 1993–2005: Synthesis and Future Directions, *Science*, 315, 612–617, <https://doi.org/10.1126/science.1131669>, 2007.

Cape, M. R., Vernet, M., Pettit, E. C., Wellner, J., Truffer, M., Akie, G., Domack, E., Leventer, A., Smith, C. R., and Huber, B. A.: Circumpolar Deep Water Impacts Glacial Meltwater Export and Coastal Biogeochemical Cycling Along the West Antarctic Peninsula, *Front. Mar. Sci.*, 6, <https://doi.org/10.3389/fmars.2019.00144>, 2019.

Cavalieri, D. J., Parkinson, C. L., Gloersen, P., and Zwally, H. J.: Sea Ice Concentrations from Nimbus-7 SMMR and DMSP SSM/I-SSMIS Passive Microwave Data. (NSIDC-0051, Version 1), Boulder, Colorado USA, NASA National Snow and Ice Data Center Distributed Active Archive Center [data set], <https://doi.org/10.5067/8GQ8LZQVL0VL>, 1996.

Death, R., Wadham, J. L., Monteiro, F., Le Brocq, A. M., Tranter, M., Ridgwell, A., Dutkiewicz, S., and Raiswell, R.: Antarctic ice sheet fertilises the Southern Ocean, *Biogeosciences*, 11, 2635–2643, <https://doi.org/10.5194/bg-11-2635-2014>, 2014.

Dinniman, M. S., St-Laurent, P., Arrigo, K. R., Hofmann, E. E., and van Dijken, G. L.: Analysis of Iron Sources in Antarctic Continental Shelf Waters, *J. Geophys. Res. Oceans*, 125, <https://doi.org/10.1029/2019JC015736>, 2020.

Dinniman, M. S., St-Laurent, P., Arrigo, K. R., Hofmann, E. E., and van Dijken, G. L.: Sensitivity of the Relationship Between Antarctic Ice Shelves and Iron Supply to Projected Changes in the Atmospheric Forcing, *J. Geophys. Res. Ocean.*, 128, e2022JC019210, <https://doi.org/10.1029/2022JC019210>, 2023.

Dotto, T. S., Naveira Garabato, A. C., Bacon, S., Holland, P. R., Kimura, S., Firing, Y. L., Tsamados, M., Wåhlin, A. K., and Jenkins, A.: Wind-Driven Processes Controlling Oceanic Heat

Delivery to the Amundsen Sea, Antarctica, JPO, 49, 2829–2849, <https://doi.org/10.1175/JPO-D-19-0064.1>, 2019.

Douglas, C. C., Briggs, N., Brown, P., MacGilchrist, G., and Naveira Garabato, A.: Exploring the relationship between sea ice and phytoplankton growth in the Weddell Gyre using satellite and Argo float data, *Ocean Sci.*, 20, 475–497, <https://doi.org/10.5194/os-20-475-2024>, 2024.

Dutrieux, P., De Rydt, J., Jenkins, A., Holland, P. R., Ha, H., K., Lee, S. H., Steig, E. J., Ding, Q., Abrahamsen, E. P., and Schröder, M.: Strong sensitivity of Pine Island ice-shelf melting to climate variability, *Science*, 343, 174–178, <https://doi.org/10.1126/science.1244341>, 2014.

ECCO Consortium, Fukumori, I., Wang, O., Fenty, I., Forget, G., Heimbach, P., and Ponte, R. M.: ECCO Ocean Mixed Layer Depth – Monthly Mean 0.5 Degree (Version 4 Release 4), ver V4r4. PO.DACC, CA, USA [data set], <https://doi.org/10.5067/ECG5M-OML44>, 2021.

Forsch, K. O., Hahn-Woernle, L., Sherrell, R. M., Rocanova, V. J., Bu, K., Burdige, D., Vernet, M., and Barbeau, K. A.: Seasonal dispersal of fjord meltwaters as an important source of iron and manganese to coastal Antarctic phytoplankton, *Biogeosciences*, 18, 6349–6375, <https://doi.org/10.5194/bg-18-6349-2021>, 2021.

Golder, M. R. and Antoine, D.: Physical drivers of long-term chlorophyll-a variability in the Southern Ocean, *Elem. Sci. Anth.*, 13, <https://doi.org/10.1525/elementa.2024.00077>, 2025.

Garabato, A. C. N., Forryan, A., Dutrieux, P., Brannigan, L., Biddele, L. C., Heywood, K. J., Jenkins, A., Firing, Y. L., and Kimura, S.: Vigorous lateral export of the meltwater outflow from beneath an Antarctic ice shelf, *Nature*, 542, 219–222, <https://doi.org/10.1038/nature20825>, 2017.

Gerringa, L. J. A., Alderkamp, A.-C., Laan, P., Thuróczy, C.-E., De Baar, H. J. W., Mills, M. M., van Dijken, G. L., Haren, H. van, and Arrigo, K. R.: Iron from melting glaciers fuels the phytoplankton blooms in Amundsen Sea (Southern Ocean): Iron biogeochemistry, *Deep-Sea Res. II*, 71–76, 16–31, <https://doi.org/10.1016/j.dsr2.2012.03.007>, 2012.

Gerringa, L. J. A., Alderkamp, A.-C., Laan, P., Thuróczy, C.-E., de Baar, H. J. W., Mills, M. M., van Dijken, G. L., van Haren, H., and Arrigo, K. R.: Corrigendum to “Iron from melting glaciers fuels the phytoplankton blooms in Amundsen Sea (Southern Ocean): iron biogeochemistry” (Gerringa et al., 2012), *Deep-Sea Res. II*, 177, 104843, <https://doi.org/10.1016/j.dsr2.2020.104843>, 2020.

Gledhill, M. and Buck, K.: The Organic Complexation of Iron in the Marine Environment: A Review, *Front. Microbiol.*, 3, <https://doi.org/10.3389/fmicb.2012.00069>, 2012.

Goldberg, D. N., Twelves, A. G., Holland, P. R., and Wearing, K. G.: The non-local impact of Antarctic subglacial runoff, *J. Geophys. Res. Ocean*, 128, e2023JC019823, <https://doi.org/10.1029/2023JC019823>, 2023.

Ha, H. K., Wåhlin, A. K., Kim, T.W., Lee, S. H., Lee, J. H., Lee, H. J., Hong, C. S., Arneborg, L., Björk, G., and Kalén, O.: Circulation and modification of warm deep water on the central Amundsen shelf, *JPO*, 44, 1493–1501, <https://doi.org/10.1175/JPO-D-13-0240.1>, 2014.

Hassler, C., Cabanes, D., Blanco-Ameijeiras, S., Sander, S. G., Benner, R., Hassler, C., Cabanes, D., Blanco-Ameijeiras, S., Sander, S. G., and Benner, R.: Importance of refractory ligands and their photodegradation for iron oceanic inventories and cycling, *Mar. Fresh. Res.*, 71, 311–320, <https://doi.org/10.1071/MF19213>, 2019.

Hawkins, J. R., Wadham, J. L., Tranter, M., Raiswell, R., Benning, L. G., Statham, P. J., Tedstone, A., Nienow, P., Lee, K., and Telling, J.: Ice sheets as a significant source of highly reactive nanoparticulate iron to the oceans, *Nat. Commun.*, 5, 3929, <https://doi.org/10.1038/ncomms4929>, 2014.

Hayward, A., Wright, S.W., Carroll, D., Law, C. S., Wongpan, P., Gutiérrez-Rodríguez, A., and Pinkerton, M. H.: Antarctic phytoplankton communities restructure under shifting sea-ice regimes, *Nat. Clim. Chang.* 15, 889–896, <https://doi.org/10.1038/s41558-025-02379-x>, 2025.

Herraiz-Borreguero, L., Lannuzel, D., van der Merwe, P., Treverrow, A., and Pedro, J. B.: Large flux of iron from the Amery Ice Shelf marine ice to Prydz Bay, East Antarctica, *J. Geophys. Res. Ocean.*, 121, 6009–6020, <https://doi.org/10.1002/2016JC011687>, 2016.

Hersbach, H., Bell, B., Berrisford, P., Hirahara, S., Horányi, A., Muñoz-Sabater, J., Nicolas, J., Peubey, C., Radu, R., Schepers, D., Simmons, A., Soci, C., Abdalla, S., Abellán, X., Balsamo, G., Bechtold, P., Biavati, G., Bidlot, J., Bonavita, M., De Chiara, G., Dahlgren, P., Dee, D., Diamantakis, M., Dragani, R., Fleming, J., Forbes, R., Fuentes, M., Geer, A., Haimberger, L., Healy, S., Hogan, R. J., Hólm, E., Janisková, M., Keeley, S., Laloyaux, P., Lopez, P., Lupu, C., Radnoti, G., de Rosnay, P., Rozum, I., Vamborg, F., Villaume, S., and Thépaut, J.-N.: The ERA5 global reanalysis, *Q. J. R. Meteorol. Soc.*, 146, 1999–2049, <https://doi.org/10.1002/qj.3803>, 2020.

Hosking, J. S., Orr, A., Marshall, G. J., Turner, J., and Phillips, T.: The Influence of the Amundsen–Bellingshausen Seas Low on the Climate of West Antarctica and Its Representation in Coupled Climate Model Simulations, *J. Clim.*, 26, 6633–6648, <https://doi.org/10.1175/JCLI-D-12-00813.1>, 2013.

Hosking, J. S., Orr, A., Bracegirdle, T. J., and Turner, J.: Future circulation changes off West Antarctica: Sensitivity of the Amundsen Sea Low to projected anthropogenic forcing, *Geophys. Res. Lett.*, 43, 367–376, <https://doi.org/10.1002/2015GL067143>, 2016.

Huang, B., Liu, C., Banzon, V., Freeman, E., Graham, G., Hankins, B., Smith, T., and Zhang, H.-M.: Improvements of the Daily Optimum Interpolation Sea Surface Temperature (DOISST) Version 2.1, *Journal of Climate*, 34, 2923–2939, <https://doi.org/10.1175/JCLI-D-20-0166.1>, 2021.

Jacobs, S. S., Jenkins, A., Giulivi, C. F., and Dutrieux, P.: Stronger ocean circulation and increased melting under Pine Island Glacier ice shelf, *Nat. Geo.*, 4, 519–523, <https://doi.org/10.1038/ngeo1188>, 2011.

Jena, B. and Pillai, A. N.: Satellite observations of unprecedented phytoplankton blooms in the Maud Rise polynya, Southern Ocean, *The Cryosphere*, 14, 1385–1398, <https://doi.org/10.5194/tc-14-1385-2020>, 2020.

Jenkins, A., Dutrieux, P., Jacobs, S. S., McPhail, S. D., Perrett, J. R., Webb, A. T., and White, D.: Observations beneath Pine Island glacier in West Antarctica and implications for its retreat, *Nat. Geo.*, 3, 468–472, <https://doi.org/10.1038/NGEO890>, 2010.

Jourdain, N. C., Mathiot, P., Merino, N., Durand, G., Le Sommer, J., Spence, P., Dutrieux, P., and Madec, G.: Ocean circulation and sea-ice thinning induced by melting ice shelves in

the Amundsen Sea, *J. Geophys. Res. Ocean.*, 122, 2550–2573, <https://doi.org/10.1002/2016JC012509>, 2017.

Kauko, H. M., Hattermann, T., Ryan-Keogh, T., Singh, A., de Steur, L., Fransson, A., Chierici, M., Falkenhaug, T., Hallfredsson, E. H., Bratbak, G., Tsagaraki, T., Berge, T., Zhou, Q., and Moreau, S.: Phenology and Environmental Control of Phytoplankton Blooms in the Kong Håkon VII Hav in the Southern Ocean, *Front. Mar. Sci.*, 8, <https://doi.org/10.3389/fmars.2021.623856>, 2021.

Lannuzel, D., Fourquez, M., de Jong, J., Tison, J.-L., Delille, B., and Schoemann, V.: First report on biological iron uptake in the Antarctic sea-ice environment, *Polar Biol.*, 46, 339–355, <https://doi.org/10.1007/s00300-023-03127-7>, 2023.

Lee, S. H., Kim, B. K., Lim, Y. J., Joo, H., Kang, J. J., Lee, D., Park, J., Ha, S.-Y., and Lee, S. H.: Small phytoplankton contribution to the standing stocks and the total primary production in the Amundsen Sea, *Biogeosciences*, 14, 3705–3713, <https://doi.org/10.5194/bg-14-3705-2017>, 2017.

Lee, Y., Park, J., Jung, J., and Kim, T. W.: Unprecedented differences in phytoplankton community structures in the Amundsen Sea polynyas, West Antarctica, *Environ. Res. Lett.* 17, 114022, <https://doi.org/10.1088/1748-9326/ac9a5f>, 2022.

Liniger, G., Strutton, P. G., Lannuzel, D., and Moreau, S.: Calving event led to changes in phytoplankton bloom phenology in the Mertz polynya, Antarctica, *J. Geophys. Res. Oceans*, 125, e2020JC016387, <https://doi.org/10.1029/2020JC016387>, 2020.

Liu, Y., Moore, J. C., Cheng, X., Gladstone, R. M., Bassis, J. N., Liu, H., Wen, J., and Hui, F.: Ocean-driven thinning enhances iceberg calving and retreat of Antarctic ice shelves, *Proc. Nat. Acad. Sci.*, 112, 3263–3268, <https://doi.org/10.1073/pnas.1415137112>, 2015.

Marchese, C., Albouy, C., Tremblay, J.-É., Dumont, D., D'Ortenzio, F., Vissault, S., and Bélanger, S.: Changes in phytoplankton bloom phenology over the North Water (NOW) polynya: a response to changing environmental conditions, *Polar Biol.*, 40, 1721–1737, <https://doi.org/10.1007/s00300-017-2095-2>, 2017.

Maritorena, S. and Siegel, D. A.: Consistent merging of satellite ocean color data sets using a bio-optical model, *Rem. Sens. Environ.*, 94, 429–440, <https://doi.org/10.1016/j.rse.2004.08.014>, 2005.

McClish, S. and Bushinsky, S. M.: Majority of Southern Ocean seasonal ice zone bloom net community production precedes total ice retreat, *Geophys. Res. Lett.*, 50, e2023GL103459, <https://doi.org/10.1029/2023GL103459>, 2023.

Meredith, M., Sommernorn, M., Cassotta, S., Derksen, C., Ekyakin, A., Hollowed, A., Kofinas, G., Mackintosh, A., Melbourne-Thomas, J., Muelbert, M. M. C., Ottersen, G., Pritchard, H., and Schurr, E. A. G.: Polar Regions, in: *IPCC Special Report on the Ocean and Cryosphere in a Changing Climate*, edited by: Pörtner, H.-O., Roberts, D. C., Masson-Delmotte, V., Zhai, P., Tignor, M., Poloczanska, E., Mintenbeck, K., Alegria, A., Nicolai, M., Okem, A., Petzold, J., Rama, B., and Weyer, N. M., Cambridge University Press, Cambridge, UK and New York, NY, USA, 203–320, <https://doi.org/10.1017/9781009157964.005>, 2019.

Mills, M. M., Lindsey, R. K., van Dijken, G. L., Alderkamp, C.-A., Berg, G. M., Robinson, D. H., Welschmeyer, N. A., and Arrigo, K. R.: Photophysiology in two Southern Ocean phytoplankton taxa: photosynthesis of *Phaeocystis antarctica* (prymnesiophyceae) and *fragilariopsis cylindrus* (bacillariophyceae) under simulated mixed-layer irradiance, *J. Phycol.*, 46, 1114–1127, <https://doi.org/10.1111/j.1529-8817.2010.00923.x>, 2010.

Mills, M. M., Alderkamp, C.-A., Thuróczy, C.-E., van Dijken, G. L., Laan, P., de Barr, H. J. W. and Arrigo, K. R.: Phytoplankton biomass and pigment responses to Fe amendments on the Pine Island and Amundsen polynyas, *Deep-Sea Res. II*, 71–76, 61–76, <https://doi.org/10.1016/j.dsri.2012.03.008>, 2012.

Morales Maqueda, M. A.: Polynya Dynamics: a Review of Observations and Modeling, *Rev. Geophys.*, 42, RG1004, <https://doi.org/10.1029/2002RG000116>, 2004.

Moreau, S., Mostajir, B., Bélanger, S., Schloss, I. R., Vandepol, M., Demers, S., and Ferreyra, G. A.: Climate change enhances primary production in the western Antarctic Peninsula, *Glob. Chang. Biol.*, 21, 2191–2205, <https://doi.org/10.1111/gcb.12878>, 2015.

Naughten, K. A., Meissner, K. J., Galton-Fenzi, B. K., England, M. H., Timmermann, R., and Hellmer, H. H.: Future Projections of Antarctic Ice Shelf Melting Based on CMIP5 Scenarios, *J. Clim.*, 31, 5243–5261, <https://doi.org/10.1175/JCLI-D-17-0854.1>, 2018.

Naughten, K. A., Holland, P. R., and De Rydt, J.: Unavoidable future increase in West Antarctic ice-shelf melting over the twenty-first century, *Nat. Clim. Change.*, 13, 1222–1228, <https://doi.org/10.1038/s41558-023-01818-x>, 2023.

Nunes, G. S., Ferreira, A., and Brito, A.C. Long-term satellite data reveals complex phytoplankton dynamics in the Ross Sea, Antarctica, *Commun. Earth. Environ.*, 6, 864, <https://doi.org/10.1038/s43247-025-02590-w>, 2025.

Oh, J.-H., Noh, K. M., Lim, H.-G., Jin, E. K., Jun, S.-Y., and Kug, J.-S.: Antarctic meltwater-induced dynamical changes in phytoplankton in the Southern Ocean, *Environ. Res. Lett.*, 17, 024022, <https://doi.org/10.1088/1748-9326/ac444e>, 2022.

Oliver, H., St-Laurent, P., Sherrell, R. M., and Yager, P. L.: Modeling Iron and Light Controls on the Summer *Phaeocystis antarctica* Bloom in the Amundsen Sea Polynya, *Global Biogeochem. Cycles*, 2018GB006168, <https://doi.org/10.1029/2018GB006168>, 2019.

Pan, J. B., Gierach, M. M., Stammerjohn, S., Schofield, O., Meredith, M. P., Reynolds, R. A., Vernet, M., Haumann, F. A., Orona, A. J., and Miller, C. E.: Impact of glacial meltwater on phytoplankton biomass along the Western Antarctic Peninsula, *Comm. Earth. Environ.*, 6, 456, <https://doi.org/10.1038/s43247-025-02435-6>, 2025.

Paolo, F. S., Fricker, H. A., and Padman, L.: Volume loss from Antarctic ice shelves is accelerating, *Science*, 348, 327–331, <https://doi.org/10.1126/science.aaa0940>, 2015.

Paolo, F. S., Fricker, H. A., and Padman, L.: Constructing improved decadal records of Antarctic ice shelf height change from multiple satellite radar altimeters, *Remote Sens. Environ.*, 177, 192–205, <https://doi.org/10.1016/j.rse.2016.01.026>, 2016.

Paolo, F. S., Gardner, A. S., Greene, C. A., Nilsson, J., Schodlok, M. P., Schlegel, N.-J., and Fricker, H. A.: Widespread slowdown in thinning rates of West Antarctic ice shelves, *The Cryosphere*, 17, 3409–3433, <https://doi.org/10.5194/tc-17-3409-2023>, 2023.

Park, J., Kuzminov, F. I., Bailleul, B., Yang, E. J., Lee, S., Falkowski, P. G., and Gorbulov, M. Y.: Light availability rather than Fe controls the magnitude of massive phytoplankton bloom in the Amundsen Sea polynyas, Antarctica: Light availability

rather than Fe controls phytoplankton bloom, *Limnol. Oceanogr.*, 62, 2260–2276, <https://doi.org/10.1002/lno.10565>, 2017.

Park, J., Kim, J.-H., Kim, H., Hwang, J., Jo, Y.-H., and Lee, S. H.: Environmental Forcings on the Remotely Sensed Phytoplankton Bloom Phenology in the Central Ross Sea Polynya, *J. Geophys. Res. Ocean.*, 124, 5400–5417, <https://doi.org/10.1029/2019JC015222>, 2019.

Person, R., Aumont, O., Madec, G., Vancoppenolle, M., Bopp, L., and Merino, N.: Sensitivity of ocean biogeochemistry to the iron supply from the Antarctic Ice Sheet explored with a biogeochemical model, *Biogeosciences*, 16, 3583–3603, <https://doi.org/10.5194/bg-16-3583-2019>, 2019.

Pritchard, H. D., Ligtenberg, S. R. M., Fricker, H. A., Vaughan, D. G., van den Broeke, M. R., and Padman, L.: Antarctic ice-sheet loss driven by basal melting of ice shelves, *Nature*, 484, 502–505, <https://doi.org/10.1038/nature10968>, 2012.

Racault, M.-F., Le Quéré, C., Buitenhuis, E., Sathyendranath, S., and Platt, T.: Phytoplankton phenology in the global ocean, *Ecol. Indic.*, 14, 152–163, <https://doi.org/10.1016/j.ecolind.2011.07.010>, 2012.

Randall-Goodwin, E., Meredith, M. P., Jenkins, A., Yager, P. L., Sherrell, R. M., Abrahamsen, E. P., Guerrero, R., Yuan, X., Mortlock, R. A., Gavahan, K., Alderkamp, A.-C., Ducklow, H., Robertson, R., and Stammerjohn, S. E.: Freshwater distributions and water mass structure in the Amundsen Sea Polynya region, Antarctica, *Elem. Sci. Anth.*, 3, 000065, <https://doi.org/10.12952/journal.elementa.000065>, 2015.

Rignot, E., Jacobs, S., Mouginot, J., and Scheuchl, B.: Ice-Shelf Melting Around Antarctica, *Science*, 341, 266–270, <https://doi.org/10.1126/science.1235798>, 2013.

Rignot, E., Mouginot, J., Scheuchl, B., van den Broeke, M., van Wessem, M. J., and Morlighem, M.: Four decades of Antarctic Ice Sheet mass balance from 1979–2017, *Proc. Nat. Acad. Sci.*, 116, 4, 1095–1103, <https://doi.org/10.1073/pnas.1812883116>, 2019.

Ryan-Keogh, T. J., Thomalla, S. J., Chang, N., and Moalusi, T.: A new global oceanic multi-model net primary productivity data product, *Earth Syst. Sci. Data*, 15, 4829–4848, <https://doi.org/10.5194/essd-15-4829-2023>, 2023.

Sari El Dine, Z., Guinet, C., Picard, B., Thyssen, M., Duforêt-gaurier, L., and El Hourany, R.: Influence of the phytoplankton community structure on the southern elephant seals' foraging activity within the Southern Ocean, *Commun. Biol.*, 8, 620, <https://doi.org/10.1038/s42003-025-08049-0>, 2025.

Scambos, T., Bell, R. E., Alley, R. B., Anandakrishnan, S., Bromwich, D. H., Brunt, K., Christianson, K., Creyts, T., Das, S. B., DeConto, R., Dutrieux, P., Fricker, H. A., Holland, D., MacGregor, J., Medley, B., Nicolas, J. P., Pollard, D., Siegfried, M. R., Smith, A. M., Steig, E. J., Trusel, L. D., Vaughan, D. G., and Yager, P. L.: How much, how fast?: A science review and outlook for research on the instability of Antarctica's Thwaites Glacier in the 21st century, *Glob. Planet. Change*, 153, 16–34, <https://doi.org/10.1016/j.gloplacha.2017.04.008>, 2017.

Silsbe, G. M., Behrenfeld, M. J., Halsey, K. H., Milligan, A. J., and Westberry, T. K.: The CAFE model: A net production model for global ocean phytoplankton, *Global Biogeochem. Cycles*, 30, 1756–1777, <https://doi.org/10.1002/2016GB005521>, 2016.

Shepherd, A., Ivins, E., Rignot, E., Smith, B., van den Broeke, M., Velicogna, I., Whitehouse, P., Briggs, K., Jougin, I., Krinner, G., Nowicki, S., Payne, T., Scambos, T., Schlegel, N., A. G., Agosta, C., Ahlström, A., Babonis, G., Barletta, V., Blazquez, A., Bonin, J., Csatho, B., Cullather, R., Felikson, D., Fettweis, X., Forsberg, R., Gallee, H., Gardner, A., Gilbert, L., Groh, A., Gunter, B., Hanna, E., Harig, C., Helm, V., Horvath, A., Horwath, M., Khan, S., Kjeldsen, K. K., Konrad, H., Langen, P., Lecavalier, B., Loomis, B., Luthcke, S., McMillan, M., Melini, D., Mernild, S., Mohajerani, Y., Moore, P., Mouginot, J., Moyano, G., Muir, A., Nagler, T., Nield, G., Nilsson, J., Noel, B., Otosaka, I., Pattle, M. E., Peltier, W. R., Pie, N., Rietbroek, R., Rott, H., Sandberg-Sørensen, L., Sasgen, I., Save, H., Scheuchl, B., Schrama, E., Schröder, L., Seo, K.-W., Simonsen, S., Slater, T., Spada, G., Sutterley, T., Talpe, M., Tarasov, L., van de Berg, W. J., van der Wal, W., van Wessem, M., Vishwakarma, B. D., Wiese, D., Wouters, B., and The IMBIE team: Mass balance of the Antarctic Ice Sheet from 1992 to 2017, *Nature*, 558, 219–222, <https://doi.org/10.1038/s41586-018-0179-y>, 2018.

Sherrell, R. M., Lagerström, M. E., Forsch, K. O., Stammerjohn, S. E., and Yager, P. L.: Dynamics of dissolved iron and other bioactive trace metals (Mn, Ni, Cu, Zn) in the Amundsen Sea Polynya, Antarctica, *Elem. Sci. Anth.*, 3, 000071, <https://doi.org/10.12952/journal.elementa.000071>, 2015.

Siegel, D. A., Doney, S. C., and Yoder, J. A.: The North Atlantic Spring Phytoplankton Bloom and Sverdrup's Critical Depth Hypothesis, *Science*, 296, 730–733, <https://doi.org/10.1126/science.1069174>, 2002.

Smith, A. J. R., Nelson, T., Ratnarajah, L., Genovese, C., Westwood, K., Holmes, T. M., Corkill, M., Townsend, A. T., Bell, E., Wuttig, K., and Lannuzel, D.: Identifying potential sources of iron-binding ligands in coastal Antarctic environments and the wider Southern Ocean, *Front. Mar. Sci.*, 9, <https://doi.org/10.3389/fmars.2022.948772>, 2022.

Soppa, M. A., Völker, C., and Bracher, A.: Diatom Phenology in the Southern Ocean: Mean Patterns, Trends and the Role of Climate Oscillations, *Remote Sens.*, 8, 420, <https://doi.org/10.3390/rs8050420>, 2016.

Stammerjohn, S. E., Martinson, D. G., Smith, R. C., and Ianuzzi, R. A.: Sea ice in the western Antarctic Peninsula region: Spatio-temporal variability from ecological and climate change perspectives, *Deep-Sea Res. II*, 55, 2041–2058, <https://doi.org/10.1016/j.dsr2.2008.04.026>, 2008.

Stoer, A. C. and Fennel, K.: Carbon-centric dynamics of Earth's marine phytoplankton, *Proc. Nat. Acad. Sci.*, 121, 45, e2405354121, <https://doi.org/10.1073/pnas.2405354121>, 2024.

St-Laurent, P., Yager, P. L., Sherrell, R. M., Stammerjohn, S. E., and Dinniman, M. S.: Pathways and supply of dissolved iron in the Amundsen Sea (Antarctica), *J. Geophys. Res. Oceans*, 122, 7135–7162, <https://doi.org/10.1002/2017JC013162>, 2017.

St-Laurent, P., Yager, P. L., Sherrell, R. M., Oliver, H., Dinniman, M. S., and Stammerjohn, S. E.: Modeling the Seasonal Cycle of Iron and Carbon Fluxes in the Amundsen Sea Polynya, Antarctica, *J. Geophys. Res. Oceans*, 124, 1544–1565, <https://doi.org/10.1029/2018JC014773>, 2019.

Tagliabue, A., Bowie, A. R., DeVries, T., Ellwood, M. J., Landling, W. M., Milne, A., Ohnemus, D. C., Twining, B. S., and Boyd, P. W.: The interplay between regeneration and scavenging fluxes drives ocean iron cycling, *Nat. Commun.*, 10, 4960, <https://doi.org/10.1038/s41467-019-12775-5>, 2019.

Tamsitt, V., England, M. H., Rintoul, S. R., and Morrison, A. K.: Residence Time and Transformation of Warm Circumpolar Deep Water on the Antarctic Continental Shelf, *Geophys. Res. Lett.*, 48, e2021GL096092, <https://doi.org/10.1029/2021GL096092>, 2021.

Tamura, T. P., Nomura, D., Hirano, D., Tamura, T., Kiuchi, M., Hashida, G., Makabe, R., Ono, K., Ushio, S., Yamazaki, K., Nakayama, Y., Takahashi, K. D., Sasaki, H., Murase, H., and Aoki, S.: Impacts of basal melting of the Totten Ice Shelf and biological productivity on marine biogeochemical components in Sabrina Coast, East Antarctica, *Global Biogeochem. Cycles*, 37, e2022GB007510, <https://doi.org/10.1029/2022GB007510>, 2023.

Thomalla, S. J., Nicholson, S. A., Ryan-Keogh, T. J., and Smith, M. E.: Widespread changes in Southern Ocean phytoplankton blooms linked to climate drivers, *Nat. Clim. Chang.*, 13, 975–984, <https://doi.org/10.1038/s41558-023-01768-4>, 2023.

Thuróczy, C.-E., Alderkamp, A.-C., Laan, P., Gerringa, L. J. A., Mills, M. M., van Dijken, G. L., De Baar, H. J. W., and Arrigo, K. R.: Key role of organic complexation of iron in sustaining phytoplankton blooms in the Pine Island and Amundsen Polynyas (Southern Ocean), *Deep-Sea Res. II*, 71–76, 49–60, <https://doi.org/10.1016/j.dsr2.2012.03.009>, 2012.

Turner, J., Hosking, J. S., Marshall, G. J., Phillips, T., and Bracegirdle, T. J.: Antarctic sea ice increase consistent with intrinsic variability of the Amundsen Sea Low, *Clim. Dyn.*, 46, 2391–2402, <https://doi.org/10.1007/s00382-015-2708-9>, 2016.

Twelves, A. G., Goldberg, D. N., Henley, S. F., Mazloff, M. R. and Jones, D. C.: Self-shading and meltwater spreading control the transition from light to iron limitation in an Antarctic coastal polynya, *J. Geophys. Res. Oceans*, 126, e2020JC016636, <https://doi.org/10.1029/2020JC016636>, 2021.

Vaillancourt, R. D., Sambrotto, R. N., Green, S., and Matsuda, A.: Phytoplankton biomass and photosynthetic competency in the summertime Mertz Glacier Region of East Antarctica, *Deep-Sea Res. II*, 50, 1415–1440, [https://doi.org/10.1016/S0967-0645\(03\)00077-8](https://doi.org/10.1016/S0967-0645(03)00077-8), 2003.

van Leeuwe, M. A., Webb, A. L., Venables, H. J., Visser, R. J. W., Meredith, M., P., Elzenga J. T. M., and Stefels, J.: Annual patterns in phytoplankton phenology in Antarctic coastal waters explained by environmental drivers, *Limnol. Oceanogr.*, 65, 1651–1668, <https://doi.org/10.1002/limo.11477>, 2020.

van Manen, M., Aoki, S., Brussaard, C. P. D., Conway, T. M., Eich, C., Gerringa, L., Jung, J., Kim, T.-W., Lee, S. H., Lee, Y., Reichehart, G.-J., Tian, H., Wille, F., and Middag, R.: The role of the Dotson Ice Shelf and circumpolar deep water as driver and source of dissolved and particulate iron and manganese in the Amundsen Sea polynya, Southern Ocean, *Mar. Chem.*, 104161, <https://doi.org/10.1016/j.marchem.2022.104161>, 2022.

Westberry, T., Behrenfeld, M. J., Siegel, D. A., and Boss, E.: Carbon-based primary productivity modeling with vertically resolved photoacclimation, *Global Biogeochem. Cycle*, 22, GB2024, <https://doi.org/10.1029/2007GB003078>, 2008.

Yager, P. L., Sherrell, R. M., Stammerjohn, S., Alderkamp, A.-C., Schofield, O., Abrahamsen, P., Arrigo, K., Bertilsson, S., Garay, L., Guerrero, R., Lowry, K., Moksnes, P.-O., Ndungo, K., Post, A., Randall-Goodwin, E., Riemann, L., Severmann, S., Thatje, S., van Dijken, G., and Wilson, S.: ASPIRE: The Amundsen Sea Polynya International Research Expedition, *Oceanogr.*, 25, 40–53, <https://doi.org/10.5670/oceanog.2012.73>, 2012.

Yager P. L., Sherrell, R. M., Stammerjohn, S. E., Ducklow, H. W., Schofield, O., Ingall, E. D., Wilson, S. E., Lowry, K. E., Willism, C. M., Riemann, L., Bertilsson, S., Alderkamp, A.-C., Dinasquet, J., Logares, R., Richert, I., Sipler, R. E., Melara, A. J., Mu, L., Newstead, R. G., Post, A. F., Swalethorpe, R., and van Dijken, G. L.: A carbon budget for the Amundsen Sea Polynya, Antarctica: Estimating net community production and export in a highly productive polar ecosystem, *Elem. Sci. Anth.*, 4, 000140, <https://doi.org/10.12952/journal.elementa.000140>, 2016.

Yu, L.-S., He, H., Leng, H., Liu, H., and Lin, P.: Interannual variation of summer sea surface temperature in the Amundsen Sea, Antarctica, *Front. Mar. Sci.*, 10, <https://doi.org/10.3389/fmars.2023.1050955>, 2023.

Zheng, Y., Heywood, K. J., Webber, B. G. M., Stevens, D. P., Biddle, L. C., Boehme, L., and Loose, B.: Winter seal-based observations reveal glacial meltwater surfacing in the southeastern Amundsen Sea, *Commun. Earth. Environ.*, 2, 1–9, <https://doi.org/10.1038/s43247-021-00111-z>, 2021.